MULTIMODAL MR IMAGING AND MACHINE LEARNING-BASED ASSESSMENT OF SPINAL CORD

A Research Proposal
Submitted to
The Temple University Graduate Board

---

in Partial Fulfillment
of the Requirements for the Degree of
DOCTOR OF PHILOSOPHY

---

by

Zahra Sadeghi Adl
Spring 2025

Examining Committee Members:

Dr. Feroze Mohamed, Department of Radiology, Thomas Jefferson University Hospital
Dr. Iyad Obeid, Department of Electrical and Computer Engineering, Temple University
Dr. Joseph Picone, Department of Electrical and Computer Engineering, Temple University
Dr. Laura Krisa, Department of Physical Therapy, Thomas Jefferson University Hospital

Abstract

Multimodal MR Imaging and Machine Learning-Based Assessment of Spinal Cord

by

Zahra Sadeghi Adl

Accurate assessment of spinal cord integrity is crucial for diagnosing abnormalities, guiding therapeutic interventions, and improving patient outcomes. While traditional T1- and T2-weighted Magnetic Resonance Imaging (MRI) sequences remain fundamental in clinical practice, they often lack the sensitivity and specificity to detect subtle microstructural changes indicative of early or progressive pathology. Advanced MRI techniques, such as Diffusion Tensor Imaging (DTI), Neurite Orientation Dispersion and Density Imaging (NODDI), Diffusion Kurtosis Imaging (DKI), and Magnetization Transfer Imaging (MTI), provide deeper insights into spinal cord tissue organization and microstructure. However, the absence of a robust, pediatric-specific normative benchmark limits their clinical utility, hindering early and accurate detection and intervention in pediatric spinal cord abnormalities, where timely treatment can significantly impact long-term neurological outcomes.

Spinal Cord Injury (SCI), a debilitating neurological condition with both acute and chronic manifestations, underscores the need for objective, automated diagnostic tools. Traditional clinical assessments, such as the American Spinal Injury Association (ASIA) Impairment Scale (AIS), rely on subjective evaluations that may overlook critical injury characteristics. This limitation can lead to delayed or suboptimal treatment decisions. Machine learning approaches offer a promising solution by leveraging high-dimensional MRI data to identify subtle patterns associated with injury severity and prognosis, thereby enhancing diagnostic precision and clinical decision-making.

This thesis proposal aims to address these challenges through a three-phase approach. First, a pediatric MRI biomarker database will be established by collecting

and analyzing structural and diffusion imaging data from 150 typically developing (TD) children. The dataset will include T1-weighted, T2-weighted, DTI, NODDI, DKI, and MTI sequences, along with demographic metadata including age, sex, and height, all acquired under standardized research protocols. Appropriate de-identification and privacy protocols will be implemented to support public release for broader research use. This will be the first comprehensive, multimodal MRI database of the pediatric spinal cord, addressing the lack of normative benchmarks and allowing for quantitative assessment of normal spinal cord development. Second, machine learning-based models will be developed to predict injury severity in pediatric patients with chronic traumatic SCI by integrating structural, diffusion, and demographic features. This will be the first study to incorporate multimodal MRI biomarkers with deep learning for chronic pediatric SCI classification, providing a robust, data-driven method for classifying injury severity based on quantitative imaging features. Finally, predictive models for acute traumatic adult SCI will be designed using multimodal MRI data, employing Convolutional Neural Networks (CNNs) with attention mechanisms to improve severity prediction and support immediate clinical interventions. While the pediatric models rely on extracted features from chronic-phase imaging, the adult models are developed using raw MRI data from the acute phase, reflecting distinct modeling strategies aligned with each cohort's data availability. This will be the first study to develop a deep learning framework that integrates both structural and diffusion MRI for acute SCI severity classification, leveraging 3D volumetric data rather than relying on 2D slices or manually extracted features. By combining advanced MRI modalities with machine learning techniques, this research aims to provide objective, quantitative tools to facilitate precise diagnosis, prognosis, and treatment planning for spinal cord disorders in both pediatric and adult populations.

TABLE OF CONTENTS

List of Abbreviations

AD Axial Diffusivity
AIS ASIA Impairment Scale
ASIA American Spinal Injury Association
AK Axial Kurtosis
AP Anterior-Posterior
AUC Area Under the Curve
CNN Convolutional Neural Network
CSA Cross-Sectional Area
CNS Central Nervous System
CSF Cerebrospinal Fluid
DKI Diffusion Kurtosis Imaging
DTI Diffusion Tensor Imaging
DWI Diffusion-Weighted Imaging
FA Fractional Anisotropy
GM Gray Matter
HYDI Hybrid Diffusion Imaging
MD Mean Diffusivity
MK Mean Kurtosis
MRI Magnetic Resonance Imaging
MTR Magnetization Transfer Ratio
MTI Magnetization Transfer Imaging
NDI Neurite Density Index
NLI Neurological Level of Injury
NMR Nuclear Magnetic Resonance
NODDI Neurite Orientation Dispersion and Density Imaging
ODI Orientation Dispersion Index
RF Random Forest
RL Right-Left
RD Radial Diffusivity
SCI Spinal Cord Injury
SCT Spinal Cord Toolbox
SVM Support Vector Machine
TD Typically Developing
WM White Matter

CHAPTER 1

Introduction

The spinal cord is a critical component of the Central Nervous System (CNS), serving as the primary conduit for transmitting motor, sensory, and autonomic signals between the brain and the rest of the body [1, 2]. It plays a pivotal role in fundamental physiological functions, including movement, sensation, respiration, and digestion. Any disruption to its structure or function, whether due to developmental abnormalities, trauma, or degenerative conditions, can result in profound neurological deficits and diminished quality of life. Thus, accurate assessment of spinal cord integrity is essential for diagnosing abnormalities, guiding therapeutic interventions, and optimizing patient outcomes [3].

Spinal Cord Injury (SCI) is one of the most severe conditions affecting the spinal cord, leading to varying degrees of motor, sensory, and autonomic dysfunction depending on the level and extent of the injury [4]. It progresses through acute and chronic phases: the acute phase involves primary mechanical damage and secondary biological processes like inflammation and neurodegeneration, while the chronic phase leads to long-term neurodegeneration, scarring, and functional impairment [5, 6]. Despite its impact, SCI severity assessment remains challenging, particularly in pediatric cases. In clinical practice, the American Spinal Injury Association (ASIA) Impairment Scale (AIS) is widely used to evaluate injury severity based on motor and sensory function, but it relies on subjective, examiner-dependent assessments [7, 8].

Magnetic Resonance Imaging (MRI) has revolutionized spinal cord evaluation by offering non-invasive, high-resolution visualization of both macrostructural and mi-

crostructural features [9–11]. Conventional T1-weighted and T2-weighted sequences remain widely used in clinical practice for detecting macrostructural abnormalities such as lesions, atrophy, and changes in cross-sectional area [12]. However, these techniques primarily provide anatomical information and lack the ability to characterize microstructural tissue changes, including axonal integrity, myelination, and neuroinflammation, key factors in understanding disease progression. Advanced MRI techniques, including Diffusion Tensor Imaging (DTI), Neurite Orientation Dispersion and Density Imaging (NODDI), Diffusion Kurtosis Imaging (DKI), and Magnetization Transfer Imaging (MTI), have been developed to overcome some of these limitations by providing quantitative insights into spinal cord microstructure [13–17]. Each of these modalities offers unique advantages; DTI provides information on water diffusion in tissues and allows visualization of white matter tract orientation and integrity, NODDI quantifies neurite density and dispersion, DKI extends beyond DTI by capturing tissue heterogeneity and characterizing non-Gaussian diffusion, which reflects complex microstructural environments such as regions with axonal beading, demyelination, or inflammation, and MTI evaluates macromolecular content such as myelin. Hybrid Diffusion Imaging (HYDI), an emerging technique, integrates multiple diffusion protocols within a single acquisition, allowing the simultaneous derivation of DTI, NODDI, and DKI metrics [18, 19].

Despite their potential, the application of advanced MRI techniques has largely been focused on adult populations, with a significant lack of pediatric-specific normative benchmarks [20, 21]. The absence of such benchmarks hinders accurate detection of spinal cord abnormalities in children, delaying necessary interventions during critical neurodevelopmental windows [22, 23]. On the other hand, both pediatric and adult SCI research lack objective, quantitative tools for injury severity assessment across different stages of injury. Current clinical assessments, such as the AIS, remain subjective and rely on manual examinations, which are prone to variability [24].

Existing machine learning applications in SCI research have been limited to segmentation tasks or predefined feature-based classification models that rely on manual extractions rather than fully automated, end-to-end learning approaches [25, 26]. To date, only one study has attempted direct image-based SCI severity assessment, but it was restricted to a single imaging modality and relied on 2D image slices, missing the richer information present in full 3D volumetric data [27]. Furthermore, to the best of our knowledge, no existing work has developed a comprehensive, multimodal machine learning model integrating structural and diffusion MRI for SCI severity assessment, leaving a significant gap in SCI research

To address these gaps, this thesis proposal outlines a three-phase approach that integrates advanced MRI techniques, quantitative imaging biomarkers, and machine learning models. In the first phase, we will establish a pediatric MRI biomarker database by collecting and analyzing structural, diffusion, and magnetization transfer imaging data from typically developing children. Quantitative biomarkers will be extracted from these sequences, including cross-sectional area (CSA), anterior-posterior (AP) width, and right-left (RL) width from structural MRI; fractional anisotropy (FA), mean diffusivity (MD), axial diffusivity (AD), and radial diffusivity (RD) from DTI; neurite density index (NDI) and orientation dispersion index (ODI) from NODDI; mean kurtosis (MK) and axial kurtosis (AK) from DKI; and magnetization transfer ratio (MTR) from MTI. All raw imaging data will be securely stored alongside the extracted biomarkers to support future analysis, reproducibility, and open science. The dataset will be made publicly available for research use following appropriate de-identification and in full compliance with existing IRB protocols and data-sharing regulations. This will be the first comprehensive, multimodal MRI database of the pediatric spinal cord, enabling the creation of age-stratified reference values.

In the second phase, we will develop machine learning-based models to predict

injury severity in chronic pediatric SCI by integrating extracted structural and diffusion biomarkers along with demographic features. This study targets long-term structural alterations and aims to enhance automated severity classification by leveraging multimodal MRI biomarkers. While acute SCI research is vital for early prognosis, acquiring high-quality MRI data in the acute phase is challenging due to clinical and logistical constraints, as patient management and urgent medical interventions take precedence over research imaging. As a result, this study focuses on chronic cases where imaging data can be acquired under more controlled conditions, allowing for a comprehensive analysis of structural and diffusion biomarkers. This will be the first study to integrate multimodal MRI biomarkers with deep learning for pediatric SCI classification, offering a novel approach to severity assessment.

Finally, in the third phase, we will develop machine learning models for acute adult SCI using multimodal MRI data, employing convolutional neural networks (CNNs) with attention mechanisms to analyze raw imaging data and predict injury severity based on AIS scores. Acute imaging is more feasible in adult populations because MRI is routinely integrated into early clinical workflows, allowing for timely and standardized acquisition. Unlike prior studies that rely on manually extracted features or 2D image slices, this work will leverage full 3D volumetric data, capturing a more comprehensive representation of spinal cord damage. This will be the first study to integrate both structural and diffusion MRI in a deep learning framework for acute SCI severity classification, offering a data-driven approach to support immediate clinical interventions and improve early decision-making. By bridging these critical gaps, this research will enable more precise, individualized patient management and improve clinical decision-making for SCI across pediatric and adult populations. The combination of advanced MRI modalities, quantitative biomarkers, and deep learning represents a transformative step toward more accurate, data-driven diagnosis.

CHAPTER 2

Background and Literature Review

This chapter lays the interdisciplinary groundwork for the project by presenting a brief overview of three core domains: spinal cord neuroanatomy and pathology, the physics and advanced methodologies of MRI, and the emerging applications of machine learning in medical imaging. Each section is intended to outline the fundamental scientific principles while highlighting their clinical relevance and potential for advancing diagnostic and therapeutic strategies.

The first section offers a concise review of the spinal cord, detailing its anatomical organization, functional roles, and the pathophysiology of SCI. It covers the basic structure of the spinal cord, including gray and white matter organization, segmental anatomy, and the mapping of dermatomes and myotomes, followed by a brief discussion of clinical assessment methods and the key events following SCI. This overview provides essential context for understanding how structural disruptions can lead to functional impairments and underscores the importance of precise anatomical characterization in both research and clinical practice.

Next, the chapter turns to MRI. In this section, we introduce the fundamental physics underlying MRI, such as nuclear magnetic resonance, relaxation processes, and spatial encoding via gradient fields, in a succinct manner. We then survey a range of MRI sequences, from T1- and T2-weighted imaging to advanced techniques like diffusion imaging and MTI. This brief overview emphasizes how each modality contributes to the visualization and quantitative assessment of tissue integrity and microstructure, which is crucial for diagnosing and monitoring spinal cord disorders.

The final section focuses on the role of machine learning in medical imaging. We provide an outline of key ML methodologies that have been successfully applied to enhance image analysis, segmentation, and classification across various clinical settings. Following this, we discuss the specific integration of ML techniques with MRI data in the context of spinal cord imaging, highlighting how these approaches can improve diagnostic accuracy, streamline clinical assessments, and yield deeper insights into the structural and functional changes associated with SCI.

2.1 Spinal Cord

The spinal cord is a critical structure of the central nervous system, serving as the primary conduit for bidirectional communication between the brain and peripheral tissues. It extends from the medulla oblongata at the base of the brainstem to the level of the first or second lumbar vertebra, where it tapers into the conus medullaris and gives rise to the cauda equina, a bundle of spinal nerve roots. Enclosed within the vertebral column and surrounded by meninges, the spinal cord is protected from mechanical injury by cerebrospinal fluid (CSF) and the bony vertebrae [1, 2].

2.1.1 Anatomy

In cross-section, the spinal cord consists of a central core of gray matter, encased by white matter, each serving distinct functions (see Figure 1). At its center lies the central canal, a small CSF-filled channel that runs the entire length of the spinal cord and plays a crucial role in nutrient transport and waste removal. The central canal is surrounded by ependymal cells, which facilitate CSF circulation and contribute to spinal cord homeostasis [28].

The gray matter, shaped like an "H" or butterfly, consists of neuronal cell bodies and is responsible for processing incoming sensory signals and generating motor outputs. It is further organized into:

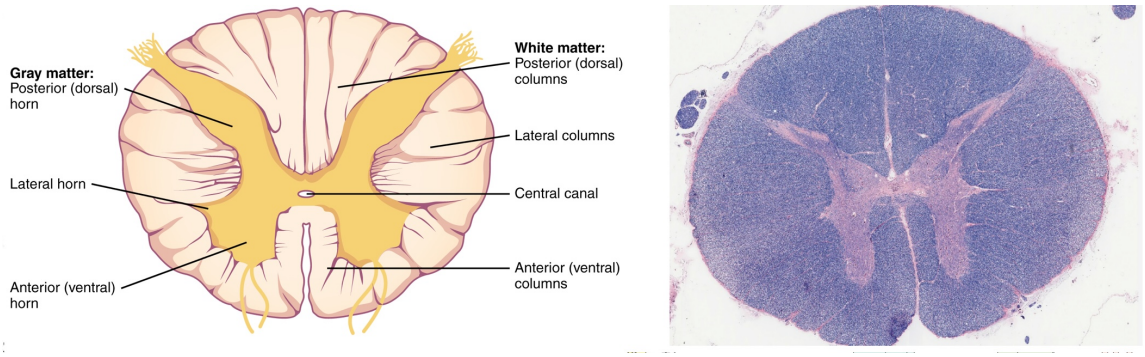

Figure 1: Cross-sectional anatomy of the human spinal cord. The left panel provides a labeled diagram highlighting the structural organization of the spinal cord, including the gray matter (dorsal, ventral, and lateral horns), white matter (posterior, lateral, and anterior columns), and the central canal. The right panel shows a histological section of the spinal cord, illustrating the distinct distribution of gray and white matter under the microscope [29].

- **Posterior (dorsal) Horns:** Contain sensory axons and interneurons involved in processing incoming sensory information.
- **Anterior (ventral) Horns:** House motor neurons that transmit motor commands to skeletal muscles.
- **Lateral Horns:** Present in the thoracic and upper lumbar regions, containing autonomic neurons that regulate sympathetic nervous system functions.

Surrounding the gray matter is white matter, which contains both myelinated and unmyelinated nerve fibers that conduct information either up (ascending) or down (descending) the spinal cord. The white matter is organized into three distinct columns:

- **Posterior (dorsal) Column:** Contains ascending sensory tracts responsible for proprioception, vibration, and fine touch.
- **Lateral Column:** Contains both ascending and descending tracts involved in voluntary movement control and pain sensation.

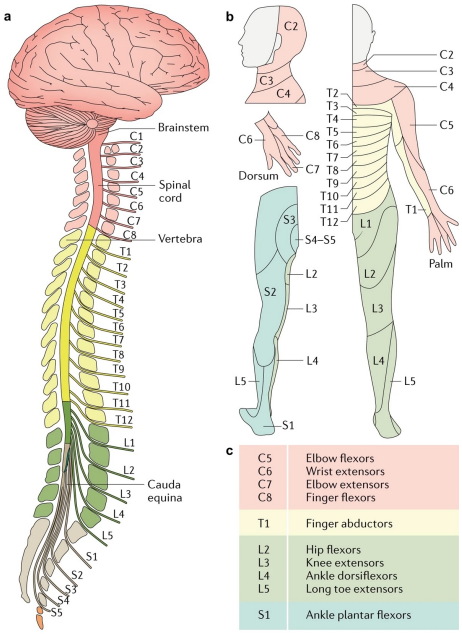

Figure 2: Anatomical and functional organization of the spinal cord. (a) Segmentation of the spinal cord into cervical, thoracic, lumbar, sacral, and coccygeal regions. (b) Dermatome map showing skin areas supplied by sensory fibers from spinal nerve roots. (c) Myotome chart highlighting key muscle groups innervated by specific spinal cord segments [30].

- **Anterior (ventral) Column:** Houses descending tracts responsible for motor control and posture.

The spinal cord is divided into five anatomically and functionally distinct regions (see Figure 2 (a)), with each region responsible for specific motor and sensory functions [30]:

- **Cervical Region (C1–C8):** Comprising eight spinal segments, the cervical region innervates the head, neck, shoulders, diaphragm, and upper limbs. The cervical enlargement (C4 to T1) supports the complex movements of the upper limbs.

- **Thoracic Region (T1–T12):** Consisting of twelve spinal segments, this region provides innervation to the thoracic and upper abdominal regions and includes

preganglionic neurons of the sympathetic nervous system within the lateral horns.

- **Lumbar Region (L1–L5):** The lumbar region, composed of five segments, innervates the lower abdominal wall and portions of the lower limbs. The lumbar enlargement, from L2 to S3, reflects the increased neural connectivity necessary to coordinate lower limb movements.

- **Sacral Region (S1–S5):** The sacral region's five segments primarily innervate the pelvic organs, perineum, and portions of the lower limbs.

- **Coccygeal Region (Co1):** This single segment contributes minimally to sensory innervation of the skin overlying the coccyx.

Each spinal cord segment provides sensory and motor innervation to specific areas of the body, known as dermatomes and myotomes, respectively. This segmental organization facilitates precise mapping of spinal cord function and helps diagnose neurological deficits resulting from injury or disease.

Dermatomes, illustrated in Figure 2 (b), correspond to specific skin areas supplied by sensory fibers from a single spinal nerve root. The cervical dermatomes (C2–C8) supply the head, neck, and upper limbs, the thoracic dermatomes (T1–T12) cover the trunk, while the lumbar (L1–L5) and sacral (S1–S5) dermatomes innervate the lower limbs and perineal region.

Myotomes refer to the muscle groups innervated by motor fibers from specific spinal cord segments. Each myotome governs distinct movements, such as elbow flexion (C5), wrist extension (C6), knee extension (L3), and ankle plantar flexion (S1), as shown in Figure 2 (c). Clinically, myotome testing is used to assess motor deficits and localize spinal cord injuries. Damage to a particular spinal segment can lead to characteristic patterns of sensory loss (dermatomal distribution) or motor

impairment (myotomal dysfunction). More severe injuries can result in complete loss of function below the injury site, profoundly impacting movement and sensation [31].

2.1.2 Spinal Cord Injury

SCI is a devastating condition with significant physical, psychological, and socioeconomic consequences. Among its types, traumatic SCI results from sudden external physical impacts such as falls, motor vehicle accidents, or acts of violence, causing immediate damage to the spinal cord [32]. This is in contrast to non-traumatic SCI, which stems from underlying conditions like tumors, infections, or degenerative diseases. In the United States, the reported incidence of traumatic spinal cord injury ranges from 28 to 55 cases per million individuals, with approximately 18,000 new cases occurring annually [33]. The primary causes include motor vehicle accidents (37.5%), falls (31.7%), acts of violence (15.4%), and sports (8%). The average age at the time of injury is 31.7 years, with the highest occurrence between ages 15 and 25, and a male-to-female ratio of 4:1. Assuming a near-normal lifespan, the estimated number of individuals living with traumatic spinal cord injury in the U.S. falls between 183,000 and 230,000 [34]. Among all spinal cord disorders, SCI demands particular attention due to its acute and long-term consequences [5].

Pathophysiology of SCI

The pathophysiology of SCI is traditionally divided into two distinct phases, acute and chronic, each presenting unique clinical challenges and requiring tailored interventions [30]. The acute phase begins immediately after the injury and is characterized by primary mechanical damage, involving the physical disruption of neural elements, blood vessels, and cell membranes. Clinically, the acute phase demands rapid and effective interventions to prevent further damage and stabilize the patient. Key priorities include restoring spinal stability, maintaining adequate blood flow to prevent

ischemia, and minimizing the effects of secondary injury cascades. Early imaging, particularly advanced MRI techniques, is crucial during this phase to assess the extent and level of injury and guide immediate clinical decisions.

The chronic phase of SCI develops weeks to months after the initial injury and is marked by long-term structural and functional changes in the spinal cord. Demyelination, resulting from the loss of myelin sheaths surrounding axons, disrupts nerve conduction and impairs signal transmission. Axonal degeneration further contributes to the permanent loss of neural connections, severely limiting the potential for functional recovery. These chronic changes solidify the long-term deficits observed in SCI patients, including motor, sensory, and autonomic impairments. In the chronic phase, clinical needs shift toward rehabilitation and functional recovery. Strategies focus on promoting neuroplasticity, minimizing secondary complications, and improving quality of life. The differing clinical needs in the acute and chronic phases emphasize the importance of timely and phase-specific interventions. In the acute phase, the primary goal is to limit secondary damage and stabilize the patient, whereas in the chronic phase, the focus shifts toward promoting recovery and improving long-term outcomes.

Clinical Assessment of SCI

Assessing the severity and functional impact of SCI is crucial for guiding treatment and predicting recovery outcomes. The most widely used clinical tool for this purpose is the American Spinal Injury Association (ASIA) Impairment Scale (AIS), which provides a standardized method for evaluating motor and sensory function [35]. The assessment involves a detailed examination of motor and sensory function to determine the neurological level of injury (NLI) and classify the injury into one of five grades, as illustrated in Figure 3:

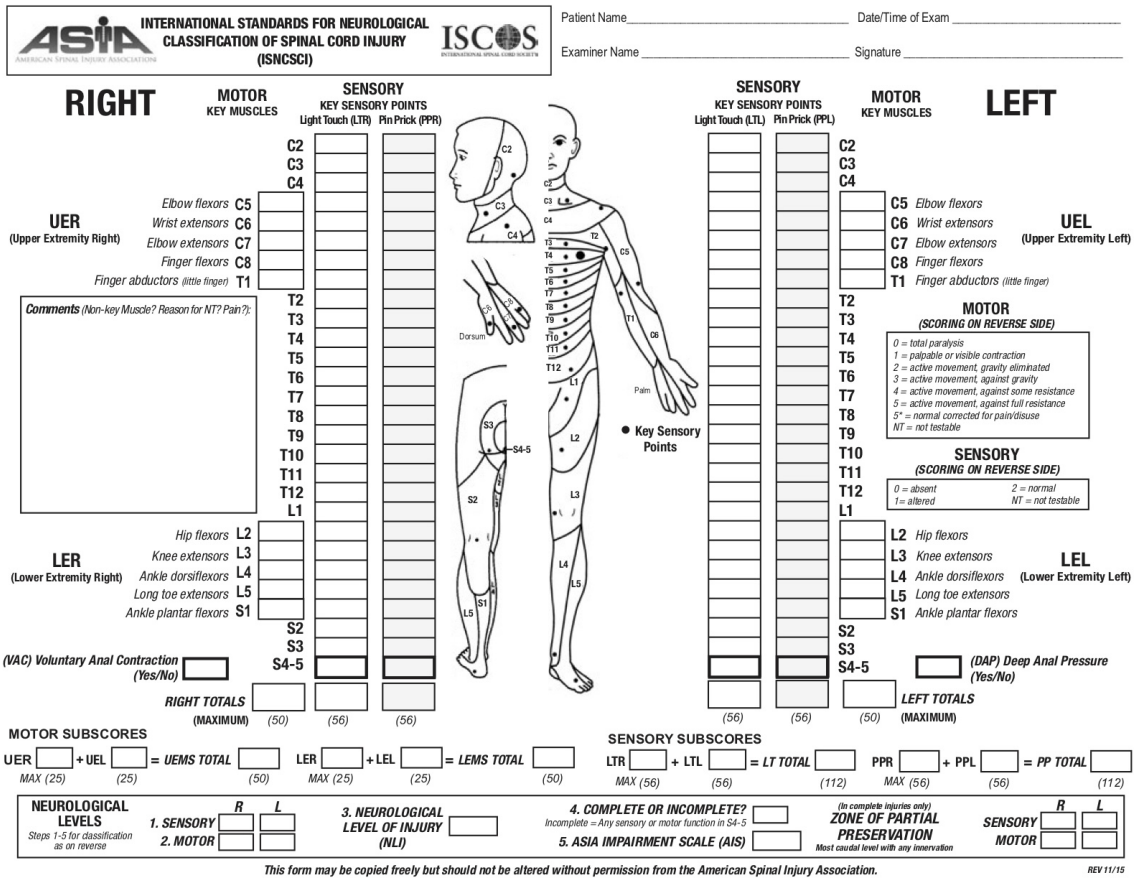

Figure 3: The AIS assessment form used for evaluating the sensory and motor function of individuals with spinal cord injury [35].

- **AIS A (Complete Injury):** No sensory or motor function is preserved below the neurological level of injury (NLI).
- **AIS B (Sensory Incomplete):** Sensory function is preserved below the NLI, but motor function is absent.
- **AIS C (Motor Incomplete):** Motor function is preserved below the NLI, but more than half of the key muscles have a strength grade less than 3.
- **AIS D (Motor Incomplete):** Motor function is preserved below the NLI, with at least half of the key muscles graded 3 or higher.
- **AIS E (Normal):** Sensory and motor functions are fully preserved.

Sensory testing is conducted bilaterally across 28 dermatomes using light touch and pinprick stimuli, scored on a 3-point scale. Motor function is assessed in 10 key muscle groups, corresponding to specific spinal levels, using a 6-point strength scale. The results are documented in a comprehensive form that includes motor and sensory scores as well as sacral sparing, which is critical for distinguishing complete from incomplete injuries.

2.2 Magnetic Resonance Imaging

MRI is a non-invasive imaging technique that has transformed neurology by providing detailed insights into the structure and function of the brain and spinal cord [11]. By utilizing the magnetic properties of hydrogen atoms, which are abundant in water and fat molecules, MRI generates high-contrast images with exceptional resolution. This capability has made it a cornerstone in modern diagnostics and research, particularly for conditions affecting the central nervous system.

2.2.1 Principles of MRI

MRI is based on the phenomenon of nuclear magnetic resonance (NMR), where atomic nuclei absorb and emit electromagnetic energy in a magnetic field [36]. Hydrogen nuclei, or protons, have an intrinsic property called spin, which creates a magnetic moment. When placed in a strong magnetic field (B_0), these protons align either parallel or antiparallel to the field, resulting in a slight net magnetization along B_0. An applied radiofrequency pulse at the Larmor frequency excites the protons, tipping the magnetization vector away from equilibrium. Once the RF pulse is turned off, the protons relax back to their original state through two distinct processes: longitudinal relaxation (T1), which describes the recovery of magnetization along B_0, and transverse relaxation (T2), which refers to the decay of magnetization in the transverse plane due to spin-spin interactions. These relaxation processes vary across tissues,

providing the contrast necessary for imaging. For instance, tissues with high water content, such as CSF, exhibit long T1 and T2 relaxation times, while fatty tissues have shorter relaxation times.

As the protons relax, they emit RF signals that are detected by receiver coils. Spatial encoding is achieved using gradient magnetic fields, which vary linearly across the body and allow the MRI system to localize the signal in three dimensions. These signals are then processed to reconstruct high-resolution images. By adjusting parameters such as repetition time (TR) and echo time (TE), MRI sequences can be optimized to emphasize specific tissue properties, making the technique highly versatile for various diagnostic applications. Beyond structural imaging, advanced MRI techniques such as diffusion imaging extend its applications to mapping neural activity and assessing tissue microstructure, further enhancing its role in understanding and treating brain and spinal conditions.

MRI sequences are specialized imaging techniques that manipulate magnetic field gradients and RF pulses to generate high-quality images with specific tissue contrast. These sequences are fundamental to the diagnosis and management of various medical conditions, as they allow clinicians to assess distinct tissue properties such as relaxation times, diffusion characteristics, and perfusion dynamics [9, 36].

Each MRI sequence is composed of a unique set of RF pulses, gradient manipulations, and signal acquisition schemes that influence image contrast and resolution. By adjusting key parameters such as TR and TE, sequences can be optimized to emphasize particular anatomical or pathological features. This versatility makes MRI an invaluable tool for assessing a wide range of conditions, from neurodegenerative diseases to musculoskeletal disorders.

2.2.2 Structural MRI

T1-Weighted Imaging

T1-weighted imaging emphasizes differences in longitudinal relaxation time (T1), which represents the time it takes for protons to exchange energy with their surrounding lattice (spin-lattice interactions) and realign with the main magnetic field after excitation by an RF pulse [12]. The longitudinal magnetization recovery follows an exponential curve described by:

$$M_z(t) = M_0 \left(1 - e^{-t/T1}\right), \tag{2.2-1}$$

where M_z is the longitudinal magnetization at time t, M_0 is the equilibrium magnetization, and T1 is the tissue-specific relaxation constant.

In T1-weighted images, tissues with shorter T1 values, such as fat, recover magnetization faster and appear bright (see Figure 4). In contrast, tissues with longer T1 values, like CSF, recover more slowly and appear dark. The key parameters for achieving T1-weighted contrast are a short TR and a short TE, ensuring that the signal depends predominantly on differences in T1. T1-weighted imaging is commonly used for anatomical visualization, especially for detecting structural abnormalities like atrophy, fibrosis, or hemorrhages.

T2-Weighted Imaging

T2-weighted imaging highlights differences in transverse relaxation time (T2), which describes the decay of transverse magnetization due to spin-spin interactions [12]. The signal decay in transverse magnetization follows:

$$M_{xy}(t) = M_0 e^{-t/T2}, \tag{2.2-2}$$

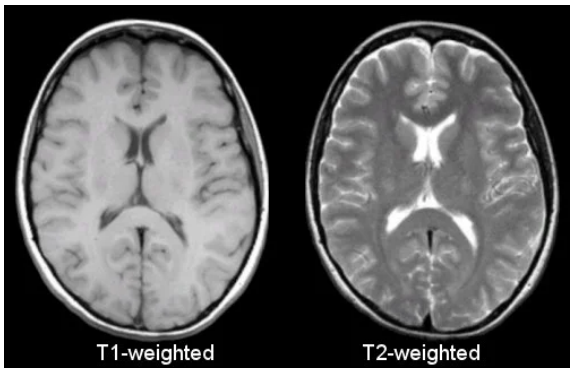

Figure 4: T1-weighted and T2-weighted MRI brain images. The T1-weighted image (left) provides high anatomical detail, with CSF appearing dark and fat appearing bright. The T2-weighted image (right) highlights fluid-rich structures, with CSF appearing bright and fat appearing dark [37].

where $M_{xy}(t)$ is the transverse magnetization at time t, and T2 is the relaxation time constant.

In T2-weighted images, tissues with longer T2 values, such as water-rich structures like CSF or regions of edema, retain transverse magnetization longer and appear bright (see Figure 4). Conversely, tissues with shorter T2 values, such as fat, decay faster and appear dark. To achieve T2-weighted contrast, long TR and TE values are used, allowing sufficient time for differences in transverse relaxation to become apparent. T2-weighted imaging is particularly valuable for detecting pathological changes involving fluid accumulation, such as edema, inflammation, syrinx formation, and demyelination. It is a cornerstone in diagnosing spinal cord injuries and neurological conditions like multiple sclerosis.

2.2.3 Diffusion MRI and Modeling Approaches

Diffusion MRI is a technique for characterizing the microstructural properties of biological tissues by measuring the displacement of water molecules. In biological tissues, water diffusion is not entirely random—it is restricted and hindered by cellular structures such as axons, myelin sheaths, and extracellular barriers. Diffusion-weighted imaging (DWI) captures this motion using magnetic field gradients that

sensitize the MR signal to molecular displacement, with different levels of sensitivity defined by the b-value. The b-value is a scalar that quantifies the strength and timing of the diffusion-sensitizing gradients applied during the MRI sequence. It reflects how much the MR signal will be attenuated due to diffusion. Higher b-values increase sensitivity to slower or more restricted diffusion, but also reduce the signal-to-noise ratio (SNR). Conversely, lower b-values are less sensitive to restricted diffusion but provide higher SNR [13].

The signal attenuation due to diffusion is described by the Stejskal-Tanner equation:

$$S = S_0 e^{-bD}, \tag{2.2-3}$$

where S is the diffusion-weighted signal, S_0 is the signal without diffusion weighting, D is the apparent diffusion coefficient (ADC), and b is the diffusion weighting factor determined by the gradient strength, duration, and timing. This formulation assumes that water molecule displacement follows a Gaussian distribution, meaning molecules diffuse equally in all directions, and their displacement probability forms a normal curve [38].

DWI serves as the foundation for various computational models that extract meaningful biological information. Several mathematical models can be applied to DWI data to capture different aspects of tissue microstructure:

Diffusion Tensor Imaging

DTI builds upon DWI by capturing both the magnitude and directionality of water diffusion [14]. While DWI measures overall diffusion, DTI represents diffusion as a tensor, a second-order symmetric 3×3 matrix that describes diffusion in three

dimensions:

$$\mathbf{D} = \begin{bmatrix} D_{xx} & D_{xy} & D_{xz} \\ D_{yx} & D_{yy} & D_{yz} \\ D_{zx} & D_{zy} & D_{zz} \end{bmatrix}. \tag{2.2-4}$$

This tensor is estimated for each voxel, capturing the local diffusion characteristics of the underlying tissue. The 3×3 structure arises from modeling diffusion along the three spatial axes (x, y, z), including interactions between them.

The eigenvalues $(\lambda_1, \lambda_2, \lambda_3)$ and eigenvectors of this tensor describe the principal diffusion directions and their magnitudes. Key metrics derived from DTI include:

- **Fractional Anisotropy (FA):** This metric quantifies the directionality of water diffusion within a voxel. Higher FA values indicate more directionally restricted diffusion, typically found in well-organized white matter tracts.
- **Mean Diffusivity (MD):** This metric represents the average magnitude of water diffusion within a voxel. Higher MD values are often associated with increased extracellular space due to tissue damage or degeneration.
- **Radial Diffusivity (RD):** This metric measures water diffusion perpendicular to the primary fiber direction. Elevated RD values are often linked to myelin degradation and demyelination.
- **Axial Diffusivity (AD):** This metric quantifies water diffusion along the primary fiber direction. Changes in AD may indicate axonal damage or degeneration.

DTI enables the mapping of white matter tracts, making it essential for studying connectivity and microstructural changes in the brain and spinal cord. DTI assumes Gaussian diffusion, which is adequate in many white matter regions but may oversimplify more complex tissue environments where non-Gaussian behavior is present.

Neurite Orientation Dispersion and Density Imaging

NODDI is a diffusion MRI technique that utilizes specially acquired diffusion data to distinguish between different water diffusion properties, allowing for the modeling of diffusion within three compartments: intracellular, extracellular, and isotropic [15]. This model enables NODDI to assess the microstructure of neurites (axons and dendrites), providing a detailed picture of neural integrity and organization. Unlike DTI, which assumes Gaussian diffusion, NODDI explicitly accounts for the underlying biological complexity of tissues by differentiating between restricted, hindered, and free water diffusion.

The NODDI model introduces three key metrics:

- **Neurite Density Index (NDI):** This metric quantifies the density of neurites by estimating the fraction of intracellular water within a voxel. A higher NDI reflects greater axonal or dendritic density, indicating intact neural architecture.
- **Orientation Dispersion Index (ODI):** ODI measures the variability in neurite orientation within a voxel. High ODI values suggest a highly dispersed arrangement, typical in areas with complex branching, while low ODI values indicate aligned fiber bundles.
- **Intracellular Volume Fraction (Vic):** Measures the proportion of free water within the tissue, often associated with extracellular fluid content.

NODDI's ability to separate isotropic diffusion, such as CSF, from anisotropic diffusion enhances its accuracy in regions where traditional DTI metrics like FA may be confounded. For instance, in spinal cord imaging, where partial volume effects from CSF are common, NODDI provides a more robust characterization of white and gray matter microstructure. Compared to DTI, NODDI offers superior specificity in detecting changes in neural density and orientation, making it highly valuable in studying neurodegeneration, neurodevelopment, and injury recovery.

Diffusion Kurtosis Imaging

DKI is designed to capture the non-Gaussian nature of water diffusion, reflecting the microstructural complexity of biological tissues [16]. While DTI assumes Gaussian diffusion, biological tissues often exhibit non-Gaussian diffusion due to barriers like cell membranes and organelles. DKI quantifies this deviation using the diffusion kurtosis coefficient, which provides additional information about tissue heterogeneity.

The signal attenuation in DKI is described by an extended Stejskal-Tanner equation:

$$S = S_0 e^{-bD+\frac{1}{6}b^2KD^2}, \tag{2.2-5}$$

where S is the diffusion-weighted signal, S_0 is the signal without diffusion weighting, K is the kurtosis coefficient, D is the diffusion coefficient, and b is the diffusion weighting factor. The term $\frac{1}{6}b^2KD^2$ arises from a Taylor expansion of the signal decay, modeling the influence of non-Gaussian effects. DKI generates several metrics, including:

- **Mean Kurtosis (MK):** Reflects the overall non-Gaussian behavior of diffusion within a voxel, providing a measure of microstructural complexity.
- **Axial Kurtosis (AK):** Describes kurtosis along the principal diffusion direction, offering insights into axonal integrity.
- **Radial Kurtosis (RK):** Quantifies kurtosis perpendicular to the principal diffusion direction, often associated with myelin sheath integrity.

DKI excels in identifying subtle microstructural changes that may not be apparent with DTI or NODDI. For instance, in spinal cord injury, DKI can detect early pathological changes such as inflammation and demyelination by capturing alterations in tissue heterogeneity. Its sensitivity to microstructural complexity makes it a valuable tool for understanding neurodegenerative diseases and assessing treatment efficacy.

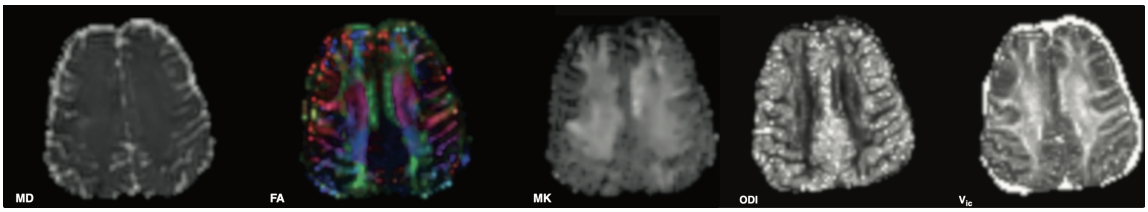

Figure 5: Example diffusion metrics of the brain. The figure illustrates MD, FA, MK, ODI, and Vic, each providing unique insights into tissue microstructure and neural organization [39].

Hybrid Diffusion Imaging

HYDI integrates the strengths of multiple diffusion models, including DTI, NODDI, and DKI, into a unified framework [18]. By combining Gaussian and non-Gaussian diffusion components, HYDI provides a comprehensive assessment of tissue microstructure, enabling a more detailed analysis of complex tissue environments.

The HYDI framework employs multi-shell diffusion imaging, which involves acquiring diffusion data at multiple b-values and directions. This multi-shell approach captures both linear (Gaussian) and non-linear (non-Gaussian) diffusion properties, allowing HYDI to extract a wide range of metrics:

- Traditional DTI metrics (e.g., FA, MD, AD, RD) for basic anisotropy and diffusivity analysis.
- NODDI-derived metrics (e.g., NDI, ODI, Vic) for compartmentalized diffusion modeling.
- Kurtosis metrics (e.g., MK, AK, RK) for non-Gaussian tissue characterization.

HYDI is particularly useful in regions with highly complex anatomy, where partial volume effects and overlapping diffusion behaviors often confound single-model approaches. By integrating multiple diffusion metrics, HYDI provides a holistic view of white and gray matter architecture, all in one acquisition, aiding in the diagnosis and monitoring of conditions like spinal cord injury and neurodegeneration. Figure 5

illustrates an example of HYDI-derived diffusion metrics, including MD, FA, MK, ODI, and Vic, demonstrating the diverse microstructural insights provided by this approach.

2.2.4 Magnetization Transfer Imaging

MTI enhances tissue contrast by exploiting the exchange of magnetization between macromolecular-bound protons (the "bound pool") and free water protons (the "free pool") [17]. An off-resonance RF pulse selectively saturates the bound pool, transferring energy to the free pool and reducing its signal intensity. This effect is quantified using the magnetization transfer ratio (MTR), calculated as:

$$\mathrm{MTR} = \frac{S_0 - S_{\mathrm{MT}}}{S_0} \times 100\% \tag{2.2-6}$$

where S_0 is the signal before the MT pulse, and S_{MT} is the signal after the MT pulse.

MTI provides valuable insights into myelin integrity, making it useful in assessing demyelinating diseases such as multiple sclerosis. Clinically, it enhances contrast in MR angiography (MRA) by suppressing background tissues, improving visualization of small vessels, and increasing the conspicuity of gadolinium-enhanced lesions in contrast-enhanced imaging [40].

2.3 Machine Learning in Medical Imaging

The integration of machine learning techniques into medical imaging has significantly enhanced image analysis by automating feature extraction, improving diagnostic accuracy, and enabling predictive modeling. Traditionally, medical image interpretation depended on handcrafted feature extraction, where radiologists and domain experts manually identified relevant features such as texture, intensity, and

shape. While these methods have been valuable, they often suffer from subjectivity, limited scalability, and suboptimal generalization across different datasets and imaging modalities. For instance, handcrafted radiomic features such as shape, intensity, and texture require expert definition and may vary significantly between annotators, leading to subjectivity and limited reproducibility [41]. Machine learning has transformed this process by enabling computational models to learn directly from imaging data and extract meaningful patterns in a more automated and data-driven manner [42].

Machine Learning techniques in medical imaging can be broadly categorized into traditional machine learning methods and deep learning approaches. Traditional Machine Learning methods have been widely used for classification, segmentation, and dimensionality reduction. These models rely on explicit feature engineering, where predefined image attributes are used as input to train predictive models. With the advancement of deep learning, more sophisticated approaches have been developed that overcome the limitations of manual feature engineering. These methods enable end-to-end learning, where models can automatically extract relevant features and make predictions without requiring explicit pre-processing.

Given the vast number of machine learning methods available, this section focuses on some of the most widely adopted and impactful techniques in medical imaging. The selection of these methods is based on their proven effectiveness in image segmentation, classification, feature extraction, and data augmentation, as well as their specific applications in medical imaging. By explaining these approaches in detail, we aim to provide a solid understanding of their theoretical foundations, mathematical formulations, and practical implications in medical imaging.

2.3.1 Traditional Machine Learning Methods

Traditional machine learning approaches have been extensively used in medical imaging for classification, segmentation, and feature selection. These models require explicit feature extraction, where domain experts define image characteristics such as texture, intensity, and shape before applying machine learning techniques.

Support Vector Machine

Support Vector Machine (SVM) is a supervised learning algorithm used for classification tasks. In SVM, the algorithm aims to find the hyperplane that best separates the data points into different classes in feature space. The hyperplane is chosen to maximize the margin, which is the distance between the hyperplane and the nearest data points from each class, also known as support vectors [43].

For linearly separable datasets, the decision boundary is represented by a hyperplane defined as:

$$f(x) = w^T x + b, \tag{2.3-7}$$

Where:$f(x)$ is the decision function, w is the weight vector, x is the input feature vector, and b is the bias term. The goal is to identify the hyperplane that maximizes the margin $\frac{2}{\|\mathbf{w}\|}$ while ensuring correct classification:

$$y_i(\mathbf{w}^T\mathbf{x}_i + b) \geq 1, \quad \forall i. \tag{2.3-8}$$

This leads to the following convex optimization problem:

$$\min_{\mathbf{w},b} \frac{1}{2}\|\mathbf{w}\|^2. \tag{2.3-9}$$

In practice, data is often not linearly separable. To address this, the soft-margin SVM introduces slack variables $\xi_i \geq 0$ that permit certain misclassifications. The

optimization objective then becomes:

$$\min_{\mathbf{w},b,\boldsymbol{\xi}} \frac{1}{2}\|\mathbf{w}\|^2 + C\sum_{i=1}^{n}\xi_i, \tag{2.3-10}$$

subject to:

$$y_i(\mathbf{w}^T\mathbf{x}_i + b) \geq 1 - \xi_i, \quad \xi_i \geq 0.$$

Here, $C \in \mathbb{R}^+$ governs the trade-off between maximizing the margin and minimizing the classification error. A larger value of C imposes a higher penalty for misclassification, leading to a narrower margin and potentially overfitting, while a smaller value allows more margin violations, promoting generalization.

SVMs have been extensively applied in medical imaging, particularly in MRI, for various diagnostic and classification tasks [44]. Their effectiveness has been demonstrated in several applications. For instance, in brain tumor classification, Gupta et al. proposed a three-step algorithm involving the identification of patients with tumors, automatic selection of abnormal slices, and segmentation and detection of the tumor [45]. Features were extracted using discrete wavelet transform on normalized images and classified by SVM, achieving a classification accuracy of 95% with 100% specificity and 90% sensitivity. Similarly, El-Dahshan et al. utilized SVMs to classify brain MRI images as normal or abnormal [46]. The authors extracted features using discrete wavelet transformation and employed kernel-based techniques, achieving high classification accuracy.

Decision Trees

Decision Trees are interpretable, non-parametric supervised learning algorithms used for both classification and regression tasks. The core principle behind decision trees is the recursive partitioning of the input feature space into subsets that become progressively more homogeneous with respect to the target variable. This is achieved

by selecting features and split points that minimize impurity at each internal node of the tree [47].

During tree construction, the algorithm evaluates candidate splits using impurity measures such as Gini impurity, which quantifies the likelihood of misclassification in classification tasks; entropy, which assesses information gain from a split; and variance reduction, commonly used in regression to reduce prediction error. Based on the chosen criterion, the data is split to form branches, and this process continues recursively until a predefined stopping condition is met. These conditions may include reaching a maximum tree depth, a minimum number of samples in a node, or achieving a pure node where all instances belong to the same class.

The resulting decision tree structure resembles a flowchart, where each internal node represents a decision rule based on a specific feature and threshold. Each branch corresponds to a decision outcome, and each leaf node contains a final prediction, either a class label in classification tasks or a numerical value in regression. This hierarchical structure allows decision trees to provide clear and interpretable decision paths, making them particularly useful in applications where model transparency is important.

Random Forest

Random Forests (RFs) are ensemble learning methods that construct multiple decision trees and aggregate their predictions [48]. Each decision tree in the ensemble is trained on a distinct bootstrap sample, which is generated by sampling with replacement from the original training dataset. To further reduce correlation between individual trees, a random subset of features is selected at each node when determining the optimal split.

For a given input $\mathbf{x}$, the prediction is obtained by majority voting (for classifica-

tion):

$$\hat{y} = \text{mode}\{h_1(\mathbf{x}), h_2(\mathbf{x}), \ldots, h_T(\mathbf{x})\},$$

where each $h_t(\mathbf{x})$ is a decision tree trained on a bootstrap sample of the data. The randomness is introduced by selecting a random subset of features at each split.

In medical imaging, RFs are often used for lesion detection and classification tasks. For disease classification, Ma et al. developed an RF-based method that integrates multiple morphological metrics to distinguish individuals with mild cognitive impairment from normal controls [49]. Utilizing voxel-based, deformation-based, and surface-based morphometry, their model achieved approximately 80% accuracy across various datasets, highlighting its robustness in early MCI diagnosis. In prognostic prediction, a study applied an RF-based random survival forest (RSF) model to MRI data for predicting progression-free survival in patients with locoregionally advanced nasopharyngeal carcinoma [50]. The RSF model, incorporating both clinical and radiomic features, showed superior predictive performance compared to traditional Cox models, suggesting its potential utility in risk stratification.

2.3.2 Deep Learning Approaches

Deep learning methods have become the dominant approach in medical imaging due to their ability to learn complex spatial representations directly from raw images [51]. Deep learning models learn hierarchical representations directly from raw data, greatly reducing the need for handcrafted features. We detail two widely used deep learning methods in medical imaging: Convolutional Neural Networks (CNNs) and Transformer-based models.

Convolutional Neural Network

Convolutional Neural Networks (CNNs) are a class of deep learning models that process image data through convolutional layers [52].

For an input image $\mathbf{X} \in \mathbb{R}^{H \times W}$ and a filter $\mathbf{F} \in \mathbb{R}^{k_h \times k_w}$, the convolution operation is defined as:

$$(\mathbf{X} * \mathbf{F})(i, j) = \sum_{m=1}^{k_h} \sum_{n=1}^{k_w} X(i + m, j + n) \cdot F(m, n),$$

where k_h and k_w denote the kernel size, and the output is a 2D feature map capturing localized spatial patterns (e.g., edges or textures).

Following the convolution, a non-linear activation function is applied to introduce non-linearity into the model. To reduce the spatial dimensions of the feature maps and improve computational efficiency, CNNs typically include pooling layers. Max pooling, for instance, replaces a local patch of values with the maximum value within that region, preserving dominant features while discarding less important ones. This downsampling step also provides some degree of translation invariance. By stacking multiple convolutional, activation, and pooling layers, CNNs build hierarchical representations of the input data, enabling them to detect low-level features in early layers and more abstract, high-level patterns in deeper layers.

Many studies have used 2D CNNs in medical imaging [53]. In the context of Alzheimer's disease detection, a study implemented and compared several deep learning models, including 2D CNNs, on 3D MRI volumes [54]. The approach involved splitting each MRI scan into 2D slices, thereby neglecting the connection among 2D image slices in an MRI volume. Similarly, another study proposed three approaches that leverage 2D CNNs on 3D MRI data for Alzheimer's disease classification [55]. The methods were tested on the Alzheimer's Disease Neuroimaging Initiative dataset across two popular 2D CNN architectures, demonstrating the potential of 2D CNNs in handling 3D MRI data for disease classification. In infant brain age classification, research explored the feasibility of using 2D CNNs on a small dataset of 3D MRI images [56]. The study found that a 2D CNN applied to central axial thick slabs achieved an accuracy of 90%. For glioma segmentation in MRI scans, a novel framework was devised that converts 3D patches into 2D slices for processing through a

2D CNN [57]. This method involved extracting 3D patches from each modality, calibrating slices via a squeeze and excitation block, and then feeding them into a 2D CNN for pixel-wise classification.

To better capture spatial context, 3D CNNs have been developed in medical imaging field. In the realm of brain tumor classification, 3D CNNs have been employed to analyze MRI volumes, capturing spatial hierarchies and contextual information inherent in the data [58]. This approach allows for the extraction of intricate features across the 3D structure, leading to improved classification performance. For instance, Mzoughi et al. (2020) proposed a deep multi-scale 3D CNN architecture for glioma brain tumor classification into low-grade and high-grade gliomas using whole volumetric T1-Gadolinium MRI sequences [59]. Their model effectively merged both local and global contextual information, resulting in enhanced classification accuracy. Similarly, a study by Anaraki et al. (2019) introduced a hybrid deep neural network combining a genetic algorithm and 3D CNN for brain tumor classification [60]. This model utilized MRI data to classify brain tumors into three types: glioma, meningioma, and pituitary tumors, demonstrating high accuracy in multi-class classification tasks.

Transformer-Based Models

Transformers are a class of deep learning models that rely on the attention mechanism to capture relationships between elements in an input sequence. Originally developed for natural language processing tasks [61], Transformers have since been successfully applied in computer vision due to their ability to model both local and global contextual dependencies.

The core component of the Transformer architecture is the attention mechanism, which allows the model to dynamically focus on the most relevant parts of the input when constructing contextualized representations. These are achieved by computing a

weighted sum over a set of input vectors, referred to as the *values*. The contribution of each value is determined by its similarity to a corresponding *query* vector, as measured against a set of *key* vectors.

Let $Q \in \mathbb{R}^{n \times d_k}$, $K \in \mathbb{R}^{n \times d_k}$, and $V \in \mathbb{R}^{n \times d_v}$ denote the query, key, and value matrices, respectively, where n is the number of input elements, d_k is the dimensionality of the query and key vectors, and d_v is the dimensionality of the value vectors. The scaled dot-product attention is computed as:

$$\text{Attention}(Q, K, V) = \text{softmax}\left(\frac{QK^\top}{\sqrt{d_k}}\right)V \tag{2.3-11}$$

In this formulation, the matrix product $QK^\top \in \mathbb{R}^{n \times n}$ contains pairwise similarity scores between each query and key. These scores are scaled by $\sqrt{d_k}$ to prevent large gradient values during training. The softmax function is applied row-wise to normalize the scores into a probability distribution, which is then used to compute a weighted sum of the value vectors. The result is a new set of representations in $\mathbb{R}^{n \times d_v}$, where each row reflects the contextualized information integrated from the rest of the sequence.

Self-attention is a special case of this mechanism in which the queries, keys, and values are all derived from the same input. Given an input sequence $X \in \mathbb{R}^{n \times d}$, self-attention begins by projecting X into three distinct subspaces using learned weight matrices:

$$Q = XW^Q, \quad K = XW^K, \quad V = XW^V, \tag{2.3-12}$$

where $W^Q, W^K, W^V \in \mathbb{R}^{d \times d_k}$ are trainable parameters. These linear projections allow the model to map the same input into query, key, and value roles. To increase the expressiveness of the model, the Transformer applies multiple self-attention operations in parallel, each referred to as a *head*, using independently learned projection weights.

The outputs of these attention heads are concatenated and passed through a feed-forward neural network.

Transformers have been increasingly adopted in medical imaging due to their ability to model long-range dependencies through self-attention mechanisms. This capability allows for capturing global context, which is particularly beneficial in complex image analysis tasks. In 2D medical imaging, transformers have been applied to various tasks, including classification and segmentation. For instance, a study implemented the Vision Transformer (ViT) architecture to classify 2D biomedical images [62]. The ViT model processes images by dividing them into patches, linearly embedding these patches, and then applying transformer layers to capture global relationships. This approach demonstrated competitive performance compared to traditional CNNs. Another approach, TransMed, combines CNNs and transformers to efficiently extract low-level features of images and establish long-range dependencies between modalities [63]. This model has been applied to multi-modal medical image classification tasks, demonstrating improved performance over traditional methods. Furthermore, the AFTer-UNet model integrates axial fusion transformers into a U-Net architecture for medical image segmentation [64]. This design captures both local and global dependencies in 2D medical images, leading to enhanced segmentation accuracy .

While most transformer-based models have been implemented in 2D settings, research on 3D transformer models remains in early stages. The UNETR model, for instance, utilizes a transformer as an encoder to learn sequence representations of input volumes, effectively capturing global multi-scale information [65]. This model connects the transformer encoder to a decoder via skip connections at different resolutions, following a U-shaped architecture. The UNETR has shown promising results in multi-organ segmentation tasks. Another notable approach is the SegFormer3D model, which introduces a lightweight and memory-efficient transformer architec-

ture for 3D medical image segmentation [66]. SegFormer3D employs a hierarchical transformer to extract multiscale volumetric features and an all-multilayer perceptron (MLP) decoder, which consists of fully connected layers that process and refine feature representations to generate segmentation masks. This design achieves a significant reduction in parameter count and computational complexity while maintaining performance.

Transformer-based architectures, while powerful, typically involve a significantly higher number of parameters compared to traditional CNNs, which makes them considerably more data-intensive. For example, the original ViT architecture contains over 85 million parameters, and 3D variants such as UNETR, designed for volumetric medical image segmentation, include approximately 91 million parameters. Although these high-capacity models offer exceptional representational power and flexibility, they also pose a substantial risk of overfitting when trained on limited datasets—an issue especially relevant in clinical research where annotated imaging data is often scarce. To address these challenges, lighter-weight architectures like SegFormer3D have been developed, typically incorporating fewer than 20 million parameters. These models aim to balance performance and computational efficiency, making them more practical for medical imaging tasks where large annotated datasets are not always available. For instance, UNETR was trained on more than 1,000 3D MRI volumes from the Medical Segmentation Decathlon (MSD) dataset, while SegFormer3D has shown strong performance on datasets comprising only 100 to 300 3D volumes.

2.3.3 Applications in SCI

Machine Learning has been increasingly applied to SCI research, with studies primarily focusing on segmentation, diagnostic classification, and prognostication [51]. While these applications have demonstrated promising results, major gaps persist, particularly in SCI severity assessment based on imaging data, the lack of 3D deep

learning methods, and insufficient multimodal approaches.

Segmentation

Segmentation has been the primary focus of Machine Learning applications in SCI, aiming to automate spinal cord and lesion delineation from MRI scans. McCoy et al. (2019) developed a 2D CNN-based segmentation model to detect spinal cord contusions in T2-weighted MRI scans [67]. This model processed individual axial slices rather than utilizing full volumetric information, limiting its ability to capture spatial injury progression across vertebral levels. The study analyzed data from a large cohort of 862 participants, of which 65% were able to walk either at discharge or at one-year follow-up, and 35% were unable to walk, based on FIM motor scores. Similarly, SCIseg, a deep learning segmentation tool, was designed for spinal cord and lesion segmentation, but it also relied on 2D processing rather than a fully 3D approach [68]. The SCIseg model was trained on MRI data from 191 SCI patients acquired from three different sites. The dataset included a heterogeneous mix of lesion etiologies (traumatic, ischemic, hemorrhagic), spinal levels (cervical, thoracic, lumbar), and acquisition protocols (axial/sagittal orientations and isotropic/anisotropic resolutions). While these methods have improved segmentation accuracy and automation, they fail to leverage 3D spatial continuity, which is crucial for comprehensive SCI analysis.

Diagnostic Classification

Machine learning models have been employed to classify SCI based on imaging and non-imaging biomarkers. However, most classification studies rely on extracted features rather than end-to-end image-based learning. For instance, Arslan et al. (2012) utilized SVM and hierarchical clustering analysis to classify SCI patients based on skin impedance rather than MRI scans [25]. Their study included 15 patients with

traumatic SCI (13 paraplegic and 2 tetraplegic) and 15 age-matched healthy control subjects between 18 and 55 years of age. Skin impedance was measured bilaterally at key dermatomal points spanning from C3 to S1, excluding certain regions (e.g., C2, L1–L3, S2–S5) due to anatomical or participant limitations. All patients had chronic traumatic SCI with a duration ranging from 3 to 20 years. Similarly, Tay et al. (2014) used SVM and k-Nearest Neighbors (KNN) classifiers to analyze FA values as predictive biomarkers, but these models were trained on precomputed features rather than raw imaging data [26]. Their study included DTI scans from 14 individuals, 9 patients with spinal cord abnormalities in the cervical region and 5 healthy controls. DTI images were generated from 26–28 axial slices spanning from the midbrain to the T1 or T2 spinal cord level, with slices outside the C1–C7 range excluded to avoid artifacts. These studies demonstrate the potential of Machine Learning for SCI classification but highlight a critical gap—current approaches largely exclude direct image-based classification, reducing their ability to generalize across different datasets and imaging protocols.

Prognostication

Predicting functional outcomes is essential for rehabilitation planning in SCI patients. Several Machine Learning models have been developed to predict AIS scores and long-term motor recovery. Okimatsu et al. (2022) implemented a CNN-based radiomics model to predict one-month neurological outcomes using MRI scans. The study retrospectively analyzed 215 patients, using a total of 294 sagittal T2-weighted MR images. These patients all had documented AIS grades at both admission and one month post-injury. However, their approach relied on extracted radiomic features rather than learning directly from imaging data [69]. Facchinello et al. (2021) used regression tree analysis to predict functional recovery based on clinical and demographic parameters [70]. Their prospective study included 172 hospitalized SCI pa-

tients, with outcomes quantified using the Spinal Cord Independence Measure (SCIM) within the first year post-injury. Predictive variables included both continuous inputs (age, Injury Severity Score, delay before surgery) and categorical features (trauma mechanism, energy of injury, neurological level, ASIA grade, early complications such as spasticity and infections). Two models were developed: a simplified model using only four predictors (age, ASIA grade, neurological level, energy of trauma), and a comprehensive model using eleven predictors.

Wiguna et al. (2024) proposed a deep learning model for SCI severity determination using axial and sagittal T2-weighted MRI scans [27]. Their study aimed to classify cervical SCI severity by segmenting the spinal cord and analyzing lesion characteristics. The dataset included MRI scans from 294 patients with traumatic and nontraumatic cervical SCI collected from 2019 to 2022. Two senior resident physicians manually labeled the images, ensuring high-quality ground truth annotations. The researchers implemented a CNN to process axial and sagittal MRI scans, using segmentation accuracy metrics such as Dice Score (0.94) and Intersection over Union (IoU, 0.89) for axial segmentation, and Dice Score (0.92) with IoU (0.85) for sagittal segmentation. Classification accuracy was evaluated using the F1 Score, achieving 0.72, with an area under the curve (AUC) of 0.79. Their model demonstrated promising results for identifying SCI severity from MRI images, but it was limited to T2-weighted MRI and used 2D images rather than a full 3D volumetric approach. While the study successfully incorporated deep learning into SCI severity assessment, it lacked multimodal integration, such as DTI or NODDI, and did not leverage 3D spatial continuity for a more comprehensive evaluation. To the best of our knowledge, this is the only study that has attempted SCI severity assessment directly from imaging data, highlighting the significant gap in existing literature. This underscores the need for future research to expand into 3D deep learning models and incorporate multiple MRI modalities to enhance SCI severity prediction.

CHAPTER 3

Research Objectives and Approach

3.1 Research Objectives

The overarching goal of this research is to advance the assessment of spinal cord integrity and injury severity through the integration of advanced multimodal MRI techniques and machine learning models. This work aims to address the critical gap in pediatric spinal cord imaging by establishing age-stratified normative quantitative MRI biomarkers, which are essential for distinguishing normal developmental changes from pathology. Furthermore, this study seeks to develop automated machine learning-based frameworks to enhance the accuracy and objectivity of SCI severity assessments, ultimately improving clinical decision-making and patient outcomes. To achieve these goals, this research is structured around the following specific aims:

Aim 1: Establish Age-stratified Normative Quantitative Structural and Hybrid Diffusion MRI Biomarker Database of the Pediatric Spinal Cord.

We will collect advanced multi-parametric MRI data, including T1-weighted, T2-weighted, HYDI, and MTI, from 150 healthy pediatric subjects aged 6 to 17 years. From the HYDI data, we will estimate DTI, NODDI, and DKI metrics, allowing us to derive key diffusion properties such as FA, MD, AD, and RD. Additionally, NODDI metrics such as NDI and ODI, as well as DKI metrics including MK and AK, will be extracted. These microstructural features, along with macrostructural metrics like CSA, AP width, and RL width, will be integrated to create a comprehensive normative database.

Aim 1 Hypothesis: We hypothesize that structural (CSA, AP, RL widths) and diffusion (FA, MD, AD, RD, NDI, ODI, MK, AK) MRI biomarkers of the pediatric spinal cord will exhibit significant linear or nonlinear correlations with age in typically developing children aged 6–17 years ($p < 0.05$).

Aim 2: Develop an Integrated Multimodal Machine Learning Framework for Automated Severity Assessment in Chronic Pediatric SCI.

Building on the normative data from Aim 1, we will integrate structural and diffusion MRI metrics with demographic variables such as age, gender, and height. Utilizing extant data from 25 pediatric SCI patients and 150 typically developing (TD) participants, we will employ machine learning algorithms to analyze the relationships between extracted imaging biomarkers and clinical outcomes, specifically AIS scores. By focusing on extracted features, this approach is optimized for the smaller dataset and allows us to leverage well-defined biomarkers for injury assessment.

Aim 2 Hypothesis: We hypothesize that a multimodal machine learning model trained on extracted structural and diffusion MRI biomarkers will predict injury severity in chronic pediatric SCI patients with statistically superior performance compared to unimodal models. The improvement will be demonstrated through cross-validated performance metrics, with statistical significance evaluated using paired t-tests or Wilcoxon signed-rank tests ($p < 0.05$).

Aim 3: Develop a Machine Learning Model for Severity Assessment Using Multi-modal MRI in Acute Adult SCI.

We will utilize CNNs enhanced with attention mechanisms to analyze raw structural MRI and DTI and clinical assessment data in the acute phase for 190 adult patients with acute SCI. Unlike Aim 2, where extracted imaging biomarkers are used due to the smaller dataset size, Aim 3 leverages the larger dataset by using raw mul-

timodal MRI images as input. By directly analyzing the spatial and microstructural information from the images, the model will predict injury severity and localization, specifically AIS scores.

Aim 3 Hypothesis: We hypothesize that an end-to-end deep learning model trained on raw multimodal MRI data from adult acute cervical SCI subjects will predict injury severity with significantly improved performance compared to single-modality models. The improvement will be demonstrated through cross-validated performance metrics, with statistical significance evaluated using paired t-tests or Wilcoxon signed-rank tests ($p < 0.05$).

3.2 Significance

Establishing a Pediatric Normative MRI Database

This study represents the first effort to establish a comprehensive pediatric spinal cord MRI biomarker database, addressing a critical gap in standardized reference values for spinal cord development. Currently, spinal cord imaging lacks pediatric-specific normative benchmarks, making it challenging to differentiate normal developmental variations from pathology [20]. By collecting multimodal MRI data (T2-weighted, DTI, NODDI, and MTI) from TD children, this project aims to provide the first large-scale dataset for spinal cord structure and microstructure in pediatrics. The normative biomarkers derived from this dataset will enable early detection of abnormalities and facilitate more precise clinical decision-making [71]. Beyond clinical applications, this unprecedented dataset will serve as a foundation for future spinal cord research, enabling novel insights into spinal cord maturation, injury response, and neurodevelopmental disorders [72].

Machine Learning for Chronic Pediatric SCI Assessment

In pediatric SCI, injury severity assessment and tracking progression over time remain challenging due to the complex interplay of demographic and clinical factors [73]. To date, no prior study has applied machine learning for SCI severity assessment in pediatric patients. Current clinical assessments rely heavily on subjective tools like the AIS, which suffer from high inter-rater variability and limited sensitivity to subtle injury-related changes [73]. This study aims to pioneer the first multimodal machine learning framework for pediatric SCI, leveraging both structural and diffusion MRI biomarkers alongside demographic factors to predict SCI severity. Existing machine learning approaches have focused on diagnostic classification but have not been used for severity grading in pediatric populations [25, 70]. To address this, our approach will integrate deep learning with quantitative MRI biomarkers, providing a more precise and objective severity assessment compared to traditional clinical evaluations. By combining multiple MRI modalities and using extracted spinal cord features, this study seeks to offer a novel predictive framework that could enhance personalized rehabilitation strategies and improve long-term patient management.

Automated Assessment for Acute Adult SCI

Acute SCI demands rapid and precise assessments to inform clinical decisions and prevent secondary complications. Traditional assessment methods often rely on visual interpretation of MRI scans, which may overlook subtle changes crucial for prognosis and treatment planning [51]. While machine learning-based approaches have been explored for acute adult SCI, only one prior study attempted image-based severity assessment, and it was limited to 2D image slices and a single MRI modality [27]. This study aims to develop the first 3D multimodal deep learning model for SCI severity classification using T2-weighted and DTI data. Unlike prior studies that relied on manually extracted imaging features, our approach will directly process raw mul-

timodal MRI data through deep learning architectures with attention mechanisms, enabling a richer representation of spinal cord pathology. By leveraging 3D volumetric data, our model seeks to capture complex spatial relationships along the spinal cord, improving accuracy and generalizability in predicting AIS severity categories. This study intends to set a new standard for automated SCI severity assessment, offering a clinically applicable model that enhances early intervention strategies and personalized treatment planning.

3.3 Approach

3.3.1 Study Population

The study population consists of both pediatric and adult subjects, categorized based on their spinal cord condition to align with the specific research aims. All data collection and retrospective data analysis have received IRB approval from Thomas Jefferson University Hospital. Sample sizes for each aim were determined based on a combination of statistical power analyses, precedent in neuroimaging literature, and requirements for robust machine learning model development, while accounting for clinical feasibility and population heterogeneity.

For Aim 1, which focuses on establishing a normative pediatric MRI biomarker database, the study will recruit 150 TD children and adolescents aged 6–17. Participants must meet specific inclusion criteria, including the absence of neurological or musculoskeletal disorders and normal age-appropriate cognitive and motor development. Subjects with MRI contraindications, such as metal implants or claustrophobia, or those with poor image quality due to motion artifacts will be excluded. A power analysis was conducted to ensure that a sample size of 150 provides sufficient statistical power for the primary analyses. For detecting gender differences in spinal cord MRI biomarkers using a two-sample t-test, this sample size achieves approximately

85% power to detect a medium effect size (Cohen's $d = 0.5$) at a significance level of $a = 0.05$, assuming an approximately balanced gender distribution. Furthermore, to evaluate associations between age and MRI biomarkers using Pearson correlation, a sample size of 150 provides 85% power to detect a medium correlation effect ($r = 0.35$) at $a = 0.05$. Therefore, the selected sample size is adequately powered to support the planned stratified analyses and to assess developmental trends across age and sex.

For Aim 2, which aims to develop an automated framework for severity assessment in chronic pediatric SCI, a total of 175 subjects will be used. This includes 25 pediatric SCI patients who have been recruited and evaluated with structural MRI and AIS motor scores, and 150 TD children, who are the same subjects recruited for Aim 1. These subjects will be categorized into three groups: TD, motor incomplete SCI, and motor complete SCI. Subjects with unrelated neurological disorders or MRI scans of insufficient quality will be excluded. Although the number of SCI subjects is modest, this reflects all available eligible cases with high-quality imaging and confirmed clinical assessments. A post hoc power analysis indicates that with 25 SCI and 25 TD subjects, we are powered (80%) to detect large effect sizes (Cohen's ≥ 0.8) at $a = 0.05$. The assumption of a large effect size is justified based on our preliminary analyses, which reveal marked structural differences between healthy and motor-impaired pediatric populations. These differences are particularly pronounced in spinal cord cross-sectional area and diffusion metrics, variables known to vary substantially between TD and SCI groups. Moreover, multiple recent deep learning studies have demonstrated effective modeling using similarly sized datasets. For instance, a CNN-based method was successfully trained for voxel placement in brain tumors using 125 glioma patients (Lee et al., 2023), and a V-Net-based model for 7T MRI synthesis was trained on just 18 paired 3T–7T scans (Cui et al., 2023)[74, 75]. Similarly, a classifier trained on 83 Traumatic Brain Injury patients and 40 controls achieved over 92.8% accuracy by leveraging data augmentation strategies [76]. These

examples support the feasibility of Aim 2's classification task with the available data.

For Aim 3, which focuses on severity assessment in acute adult cervical SCI, a total of 190 adult subjects who have been retrospectively identified and collected will be used. These participants presented to the Jefferson Hospital Emergency Department between 2010 and 2019 following acute traumatic SCI. All underwent MRI within 1–24 hours post-injury and were evaluated with complete AIS assessments, providing representation across AIS grades A through D for a four-class classification task. All imaging data were acquired as part of routine clinical care and have been repurposed for research under IRB approval. No external or public datasets will be used. Eligible participants must have acute traumatic SCI at cervical levels (C1–C8), confirmed through clinical and radiological evaluations. Exclusion criteria encompass severe comorbidities that impact spinal function and incomplete or low-quality imaging data. A one-way ANOVA power analysis with four groups (assuming a moderate effect size, f=0.55, $\alpha = 0.05$, and power = 0.8) suggests a minimum of 161 subjects, which our dataset exceeds. The assumption of a moderate-to-large effect size is reasonable, given the known structural and functional disparities across AIS grades in the acute phase of injury. Additionally, several deep learning studies have demonstrated successful model development for medical imaging tasks using datasets with fewer than 250 subjects [69, 70].

3.3.2 Data Acquisition

MRI data acquisition will follow standardized protocols to ensure uniformity and reproducibility across the study population. All imaging will be performed using a 3 Tesla Siemens Prisma MRI scanner at Jefferson Hospital, utilizing sequences optimized for spinal cord assessment. Imaging protocols differ between pediatric and adult cohorts, with pediatric subjects undergoing comprehensive multimodal imaging and adult data retrospectively collected from Jefferson's SCI archive.

For **pediatric subjects (Aim 1, and 2)**, the following sequences will be acquired:

- **T1-weighted imaging:** Acquired in two slabs covering C1 to T11 with overlap to ensure seamless stitching. Imaging parameters include TR = 2000 ms, TE = 3.72 ms, and slice thickness = 1 mm. The acquisition matrix is 192 × 260 × 320, with a 0.5 mm isotropic resolution, providing high anatomical detail.

- **T2-weighted imaging:** Performed in two slabs spanning C1 to T11 with overlap to facilitate segmentation and vertebral level labeling. Parameters include TR = 1500 ms, TE = 120 ms, and slice thickness = 0.8 mm. The acquisition matrix is 64 × 320 × 320, ensuring high spatial resolution for structural analysis.

- **HYDI:** Acquired in two slabs covering C1 to T11 with overlap to maintain consistency across levels. Data are collected with multi-shell b-values of 0, 800, 1000, and 2000 s/mm^2, using an acquisition matrix of 100 × 40 × 48 with a slice thickness of 5 mm.

- **MTI:** Acquired with and without off-resonance magnetization transfer pulses at a frequency shift of 1000 Hz. Imaging parameters include TR = 35 ms, TE = 3.13 ms, and slice thickness of 5 mm. The acquisition matrix is 256 × 256 × 22, enabling the calculation of MTR for assessing myelin integrity.

For **adult subjects (Aim 3)**, MRI data will be retrospectively collected from Jefferson's SCI archive, including patients with acute cervical SCI (within 1–24 hours post-injury). The following sequences will be extracted:

- **T2-weighted imaging:** Acquired in one slab covering C1 to T1, with TR = 1500 ms, TE = 120 ms, and 0.8 mm isotropic resolution. The acquisition matrix is 256 × 256 × 58, ensuring high anatomical precision.

- **DTI:** Performed in one slab covering C1 to T1, with 32 diffusion directions and a b-value of 800 s/mm^2. The acquisition matrix is $256 \times 256 \times 58$.

Additionally, all pediatric SCI subjects will undergo the AIS assessment on the day of their MRI scan, while the assessment has already been completed for adult SCI subjects at the day of their MRI scan. This evaluation provides crucial clinical data, enabling direct correlation between neuroimaging biomarkers and functional impairment.

3.3.3 Pediatric Data Preprocessing and Feature Extraction

The data preprocessing pipeline is designed to ensure consistency, accuracy, and reproducibility of extracted quantitative MRI features across different imaging modalities. The pipeline is divided into three main stages: (1) Structural Image Preprocessing, which processes T1- and T2-weighted images for anatomical reference and structural biomarker extraction; (2) Diffusion Image Preprocessing, which processes HYDI data to extract advanced diffusion metrics; and (3) MTI Preprocessing, which computes MTR values to assess myelin integrity. All preprocessing steps align the data to the T2-weighted structural reference, enabling region-specific feature extraction from C1 to T11.

Structural Image Preprocessing: T1- and T2-Weighted Images

T1- and T2-weighted images serve as the **structural reference** for all other imaging modalities, providing a foundation for extracting morphometric features and enabling the alignment of advanced imaging sequences. The preprocessing pipeline, as shown in Figure 6, follows these steps:

1. **Stitching of Multi-Slab Acquisitions:** Since T1 and T2 acquisitions are collected in multiple slabs to optimize resolution and coverage, we first stitch

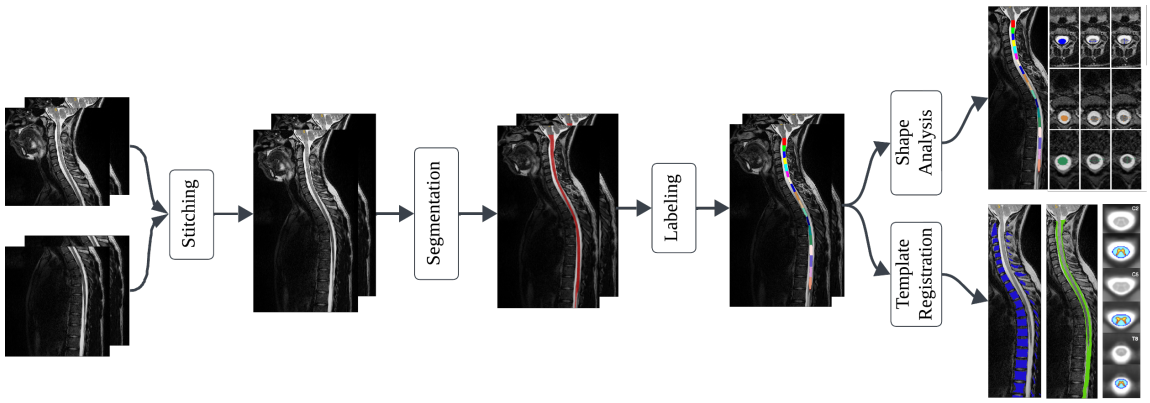

Figure 6: Pediatric Structural MRI preprocessing pipeline including stitching, segmentation, and vertebral labeling (C1–T11). Shape analysis extracts morphometric features, while template registration aligns data to the PAM50 spinal cord template for standardized analysis.

the slabs together into a continuous spinal cord volume. This ensures that the entire cervical and upper thoracic spinal cord (C1–T11) is available for segmentation and analysis.

2. **Automated Spinal Cord Segmentation:** The Spinal Cord Toolbox (SCT) is used to segment the spinal cord from surrounding tissues [77]. Two segmentation methods are applied, and a quality control step ensures that the best segmentation result is selected for further analysis.

3. **Vertebral Level Labeling:** Vertebral levels from C1 to T11 are assigned. This step ensures consistent feature extraction across all subjects.

4. **Registration of PAM50 Template to Structural Images:** To enable standardized anatomical analysis, each subject's T2-weighted spinal cord image is registered to the PAM50 spinal cord template using the SCT [77, 78]. The registration process begins with automatic centerline detection, leveraging a deep learning-based model trained to accurately localize the spinal cord center. A rigid transformation is first applied to correct for gross differences in position and orientation between the subject image and the PAM50 template, followed

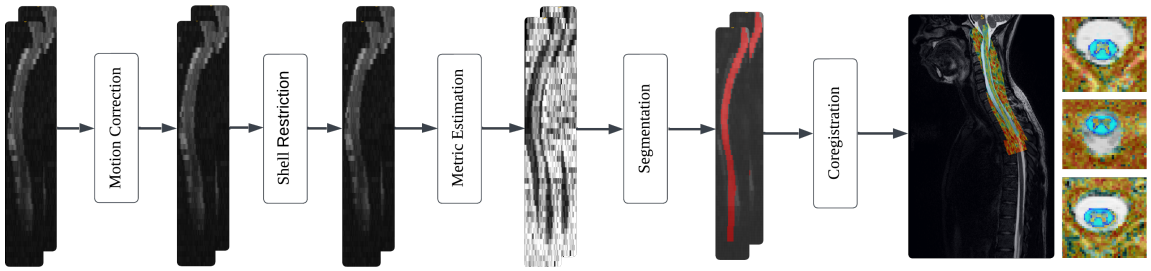

Figure 7: Diffusion MRI Processing Pipeline for Spinal Cord Imaging. The pipeline includes motion correction, shell restriction, and tensor estimation to derive FA for a single slab. Segmentation and coregistration align FA maps to the T2-weighted image and PAM50 template. FA values are extracted per vertebral level, then aggregated across slabs for C1–T11 coverage. The same process applies to other diffusion metrics.

by an affine transformation to account for inter-subject differences in scale and shear. Subsequently, a slice-wise nonlinear registration is performed along the spinal cord axis to finely warp each axial slice to the corresponding region of the template, allowing for localized anatomical alignment [79]. This allows us to bring all extracted features into a common anatomical space and generate white matter (WM), gray matter (GM), and cerebrospinal fluid (CSF) masks for precise tissue-based analyses.

5. **Extraction of Structural MRI Features:** From the preprocessed and labeled T2-weighted images, we extract key morphometric biomarkers at each vertebral level (C1–T11), including CSA, AP diameter, and RL diameter.

Diffusion Image Preprocessing: HYDI

The preprocessing pipeline for HYDI data includes the following steps:

1. **Motion Correction:** Datasets are corrected for subject motion and eddy current distortions to ensure accurate alignment of diffusion-weighted images.

2. **Shell Restriction:** The relevant shells in the HYDI dataset are used to estimate DTI, NODDI, and DKI images, each of which provides unique insights

into spinal cord microstructure.

3. **Tensor/Metric Estimation:** From the diffusion models, we estimate the following metrics: DTI metrics include FA, MD, AD, and RD; NODDI metrics include NDI and ODI; and DKI metrics include MK, AK, and RK.

4. **Segmentation and Coregistration:** Each diffusion-derived metric is segmented to isolate the spinal cord and registered to the T2-weighted image. This ensures that all features are analyzed in the T2 space and aligned with the PAM50 template for standardized analysis.

5. **Extraction at Each Vertebral Level:** After coregistration, all extracted parameters (FA, MD, AD, RD, NDI, ODI, MK, AK, and RK) are quantified at each vertebral level from C1 to T11.

Figure 7 illustrates the processing pipeline for a single imaging slab, specifically for FA extraction as an example. The same pipeline is applied to the second slab, and the results are aggregated to generate a complete C1 to T11 dataset. Additionally, this process is identical for extracting other diffusion tensor metrics (e.g., MD, AD, RD) as well as NODDI and DKI estimates, ensuring a comprehensive analysis of spinal cord microstructure.

MTI Preprocessing

The preprocessing pipeline for MTI includes the following steps:

1. **Correction for B0/B1 Field Inhomogeneities:** Spatial variations in the magnetic field are corrected to ensure accurate magnetization transfer ratio (MTR) calculations.

2. **Segmentation and Coregistration:** MTI images are aligned to the T2-weighted image and segmented to isolate spinal cord regions. This step ensures

that MTR values are computed within the spinal cord boundaries.

3. **MTR Computation:** The MTR is calculated at each vertebral level, providing a quantitative measure of myelin content and macromolecular integrity.

By applying this rigorous preprocessing pipeline, all extracted quantitative MRI metrics are aligned to the T2 structural reference, allowing precise region-specific feature extraction from C1 to T11.

3.3.4 Adult Data Preprocessing

For Aim 3, the preprocessing pipeline is designed to prepare T2-weighted and DTI data for image-based machine learning models. Unlike the pediatric pipeline, feature extraction is not performed directly; instead, the preprocessed images are used as inputs for training deep learning models. The pipeline consists of the following steps:

1. **DTI Motion Correction:** DTI datasets are corrected for subject motion and eddy current distortions to ensure accurate alignment of diffusion-weighted images.

2. **DTI Feature Extraction:** FA, MD, AD, and RD are computed from the DTI data.

3. **DTI and T2 Segmentation:** The spinal cord is segmented from surrounding tissues in all images.

4. **DTI and T2 Registration:** The DTI-derived metrics (FA, MD, AD, RD) are registered to the corresponding T2-weighted image. This ensures that all data is analyzed in the T2 space.

Figure 8 illustrates the preprocessing steps for FA extraction, following a structured workflow to ensure consistency and accuracy. The same pipeline is applied to all other diffusion metrics, including MD, AD, and RD.

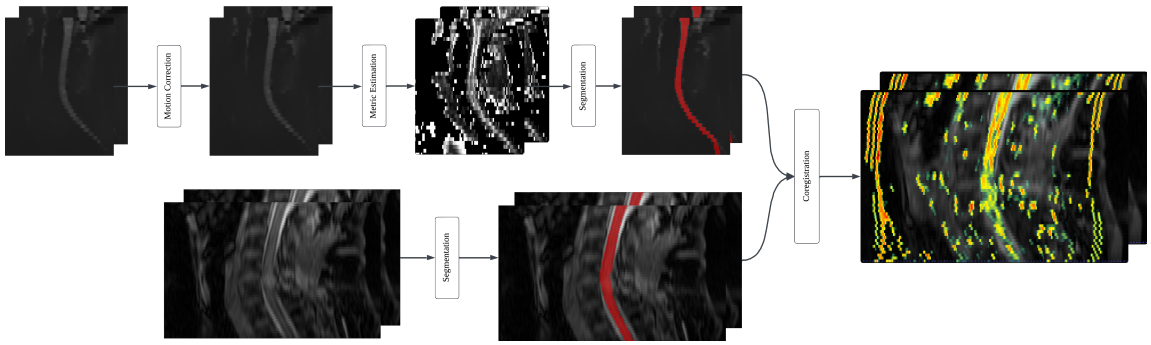

Figure 8: Adult Spinal Cord MRI Preprocessing Pipeline. The figure illustrates the pipeline for FA extraction, with the same steps applied to other diffusion metrics (MD, AD, RD). The process includes motion correction, feature extraction, segmentation, and registration to align all metrics to the T2-weighted image for deep learning model training.

3.3.5 Statistical Analysis

The statistical analysis will focus on establishing normative quantitative MRI biomarkers for the pediatric spinal cord, supporting Aim 1 of this study. The extracted features from T2-weighted imaging, diffusion models (DTI, NODDI, and DKI), and MTI will be analyzed at each vertebral level from C1 to T11. Extracted features will be reported separately for each age group, allowing for a detailed assessment of spinal cord development across childhood and adolescence.

For each MRI-derived parameter, means, standard deviations, and confidence intervals will be computed for every age group (6–17 years). These statistics will be further stratified by sex to account for anatomical and demographic variations. The extracted values will be presented in tabular format summarizing age-specific distributions and illustrated using line plots to visualize trends in spinal cord maturation.

To assess significant differences in MRI biomarkers across age groups and between sexes, data distributions will be evaluated using the Shapiro–Wilk test. Depending on normality, parametric tests (one-way ANOVA, t-tests) or non-parametric tests (e.g., Kruskal–Wallis, Mann–Whitney U) will be conducted.

Associations between continuous demographic variables (age, height) and MRI

biomarkers will be analyzed using Pearson correlation for normally distributed data and Spearman's rank correlation otherwise. Multiple linear regression models will be used to assess joint effects of demographic predictors (age, height, sex) on MRI outcomes, controlling for potential confounders. Results will be considered statistically significant at p ¡ 0.05, and effect sizes will be reported to interpret the magnitude of effects and practical significance of observed effects.

3.3.6 Machine Learning Model Development

To develop an automated framework for AIS severity assessment, machine learning models will be tailored to the extracted biomarkers for pediatric SCI (Aim 2) and imaging data for adult SCI (Aim 3). These models will leverage CNNs and attention mechanisms to classify spinal cord injury severity based on structural and diffusion-derived quantitative features or directly from MRI images.

For Aim 2, our objective is to classify AIS severity into two categories, motor complete (AIS A, B) and motor incomplete (AIS C, D), by leveraging a set of quantitative imaging features extracted from spinal cord data. The imaging features consist of structural measurements and diffusion metrics derived from T2-weighted and DTI images, respectively. Specifically, the structural features include the CSA, AP width, and RL width obtained from T2-weighted images. The diffusion metrics include FA, MD, AD, and RD. These features are extracted at each vertebral level from C1 to T11, yielding a feature matrix that encapsulates the spatial distribution of both the spinal cord's morphology and its microstructural integrity.

Initially, the extracted imaging features are organized into a feature matrix $\mathbf{X} \in \mathbb{R}^{L \times F}$, where L denotes the number of vertebral levels (e.g., $L = 11$ for C1 through T11) and F is the number of imaging features per level (with $F = 7$ in this case). This matrix serves as the sole input to the first stage of our model, which is designed to learn the spatial relationships along the spinal axis.

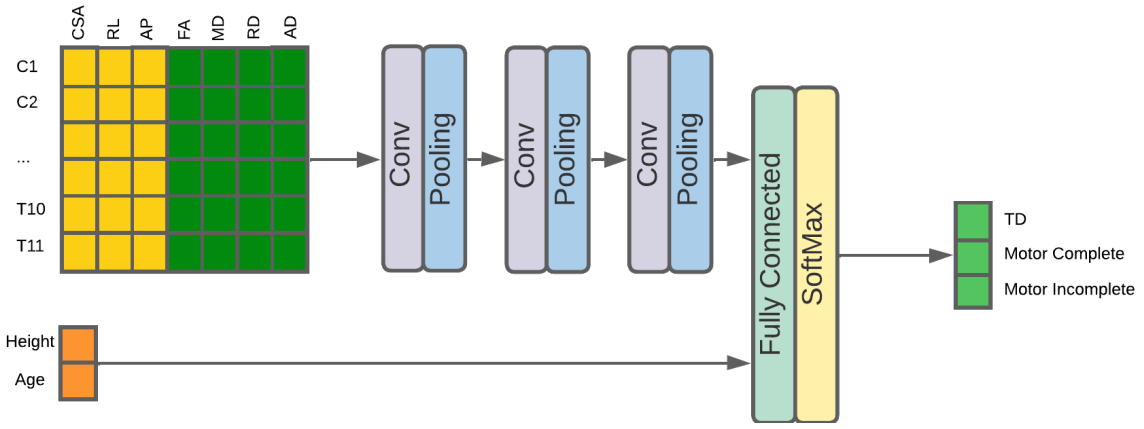

Figure 9: CNN Architecture for Aim 2 - Automated Severity Assessment in Pediatric SCI. The proposed framework for processes extracted structural and diffusion features along C1 to T11 through multiple convolutional and pooling layers to extract hierarchical features. These extracted features are then combined with demographic information and passed through fully connected layers to predict the severity of SCI.

To capture these spatial dependencies, a one-dimensional (1D) CNN is employed. The 1D CNN processes the feature matrix as a sequential signal along the vertebral levels. Pooling layers are interleaved between convolutional layers to downsample the feature maps, thereby increasing the receptive field and capturing both local and global patterns across spinal levels.

Following the convolution and pooling stages, the resulting high-level feature maps are flattened into a one-dimensional feature vector. At this point, the demographic information including age, gender, and height is concatenated to the CNN-derived feature vector. This approach ensures that the rich spatial information extracted from the imaging data is augmented with important patient-specific factors, thereby providing a more comprehensive representation for classification.

The combined feature vector is then forwarded to a series of fully connected layers that serve to integrate the information from both the imaging and demographic domains. The final layer of the network employs a softmax activation function to produce a probability distribution over the two AIS categories (motor complete and

motor incomplete) and TD. The overall architecture for Aim 2 is illustrated in Figure 9.

To address class imbalance and improve model generalizability, data augmentation techniques are applied during training. Specifically, Gaussian noise injection, where random noise sampled from a Gaussian distribution is added to the imaging features, and feature scaling are employed to simulate measurement variability and enhance the diversity of training samples. Depending on the degree of imbalance, additional strategies such as weighted loss functions, or oversampling of minority classes may be implemented to ensure robust performance across all categories. Furthermore, regularization techniques, including dropout in fully connected layers and L2 regularization (weight decay), are used to mitigate overfitting. Model parameters are optimized using an adaptive optimization algorithm that dynamically adjusts the learning rate throughout training.

For Aim 3, we propose a comprehensive 3D multimodal deep learning model to classify AIS grades (A, B, C, D) from coregistered T2-weighted and DTI images (including FA, MD, AD, and RD maps). The overarching objective is to capture both the global spatial context and the fine microstructural characteristics of the spinal cord. The input data consist of a composite volumetric dataset where each voxel is represented by multiple channels corresponding to different imaging contrasts. Specifically, the input volume $\mathbf{X} \in \mathbb{R}^{H \times W \times D \times C}$, has spatial dimensions H, W, D and C channels (with $C = 5$ representing T2, FA, MD, AD, and RD). Prior coregistration of the T2 and DTI images ensures that each voxel is spatially aligned across modalities, which is critical for accurately capturing the anatomical and microstructural details of the spinal cord.

Given the high dimensionality of the 3D data and the potential for redundant information, an autoencoder is integrated into the model to perform dimensionality reduction and feature compression. In our approach, the encoder $f_\theta(\cdot)$ is constructed

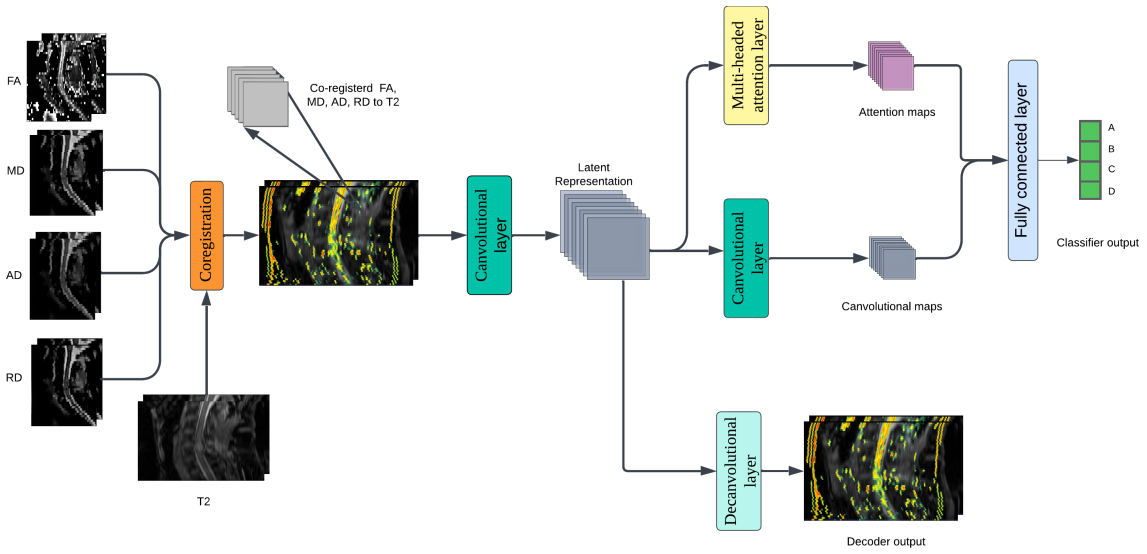

Figure 10: Deep Learning Framework for Aim 3 - Severity Assessment in Acute Adult SCI. The proposed model integrates multimodal MRI data through a deep learning pipeline. A convolutional encoder extracts hierarchical spatial representations, followed by a multi-headed attention mechanism to capture long-range dependencies. A fully connected layer then classifies injury severity, while a deconvolutional layer enables feature reconstruction for interpretability.

using several 3D convolutional layers with non-linear activation functions (e.g., ReLU) that progressively reduce the spatial dimensions while increasing the feature depth. This transformation results in a compact latent representation $\mathbf{z} = f_\theta(\mathbf{X}), \quad \mathbf{z} \in \mathbb{R}^{h \times w \times d \times k}$, where $h \ll H$, $w \ll W$, $d \ll D$, and k denotes the number of latent feature channels. During a pretraining phase, a decoder is employed to reconstruct the input from $\mathbf{z}$. This step ensures that the latent space effectively captures the most salient and discriminative features while discarding noise and redundancy.

Following dimensionality reduction, the latent representation is fed into a 3D CNN that extracts hierarchical spatial features. The 3D CNN comprises a series of convolutional layers that apply volumetric filters to learn local patterns and textures. These convolutional layers are interleaved with 3D pooling layers, which gradually reduce the spatial resolution of the feature maps and allow the network to capture more abstract, global features indicative of the spinal cord's structural integrity. This

hierarchical feature extraction is fundamental to learning both low-level details and high-level anatomical structures relevant to AIS classification.

To further enhance model interpretability and to ensure that the network emphasizes clinically pertinent regions, an attention mechanism is incorporated. A dedicated attention subnetwork processes the CNN-derived feature maps and produces a 3D attention map using additional convolutional layers followed by a softmax activation function. This attention map is then applied via element-wise multiplication, which effectively amplifies regions with high clinical relevance while suppressing less informative areas.

Subsequently, the refined feature maps are flattened and passed through one or more fully connected layers to aggregate the extracted features. The final classification layer utilizes a softmax activation function to output a probability distribution over the four AIS grades. The network is trained using a cross-entropy loss function.

To mitigate overfitting and improve generalizability, regularization techniques are applied throughout the network. Batch normalization is implemented after convolutional layers to stabilize the training process, dropout is introduced in the fully connected layers to reduce co-adaptation among neurons. The optimization is carried out using an adaptive algorithm which dynamically adjusts the learning rate based on the gradients during training. This framework aims to enhance automated severity assessment in acute spinal cord injury by leveraging multimodal MRI data, deep feature extraction, and attention mechanisms, as illustrated in Figure 10.

3.3.7 Ethical Considerations

Ethical considerations are paramount in this study to ensure compliance with institutional guidelines and protect participant welfare. All study procedures will adhere to the principles outlined in the Declaration of Helsinki and will be reviewed and approved by Institutional Review Boards (IRBs) at participating institutions. In-

formed consent will be obtained from all participants or their legal guardians prior to enrollment, with detailed explanations of study objectives, procedures, and potential risks.

To maintain participant confidentiality, all MRI and clinical data will be anonymized and stored in a secure database with restricted access. Participants will have the right to withdraw from the study at any time without consequences. Special attention will be given to ensuring the ethical inclusion of pediatric participants, with assent obtained in addition to parental consent. Regular monitoring and compliance checks will be conducted to uphold ethical standards throughout the study duration.

CHAPTER 4

Preliminary Results and Future Works

This chapter presents the preliminary results obtained from the ongoing study across all three specific aims, along with the planned future work. The analyses performed thus far provide insights into normative spinal cord structure in pediatric populations, machine learning-based classification of pediatric SCI, and preprocessing of acute adult SCI data for future classification tasks.

Aim 1: Establishing Normative Pediatric MRI Biomarker Database

To date, we have collected MRI data from 127 TD pediatric subjects. The demographic distribution of the TD cohort is summarized in Figure 11. The cohort includes 72 females and 55 males, with ages ranging from 6 to 17 years. For all scanned subjects, T2-weighted and DTI images were analyzed to extract quantitative biomarkers, including structural metrics (CSA, AP width, RL width) and diffusion metrics (FA, MD, AD, RD). Figures 12 and 13 illustrate an example analysis for a single subject. These measurements were extracted across C1 to T11 vertebral levels using the SCT toolbox [77]. Statistical analyses examined the influence of age and gender on spinal cord dimensions. We assessed correlations between CSA, AP Width, and RL Width with age and gender at each vertebral level. The analysis revealed strong age-related correlations for CSA and RL width across upper cervical levels. For instance, at vertebral level C1, CSA showed a correlation coefficient of r = 0.50 ($p < 0.0001$), and RL width r = 0.41 ($p = 0.001$). Similarly, at C2, CSA

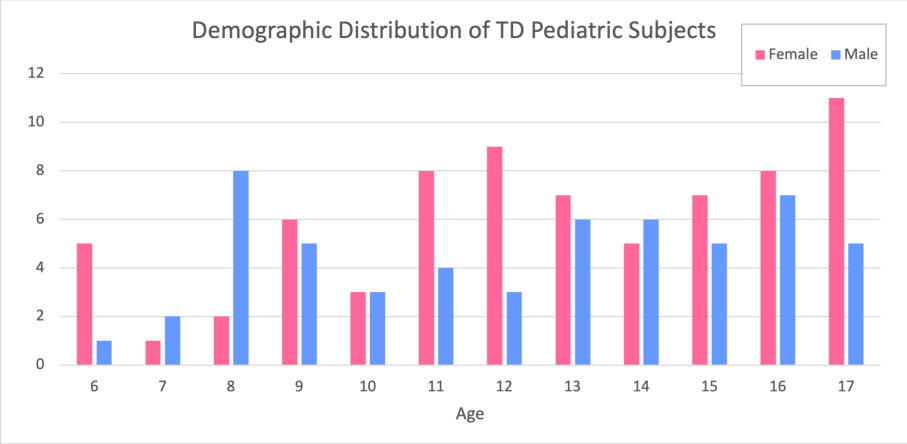

Figure 11: The distribution of TD pediatric subjects by age (6–17 years) and sex (female and male). The total number of subjects is 127, with 72 females and 55 males.

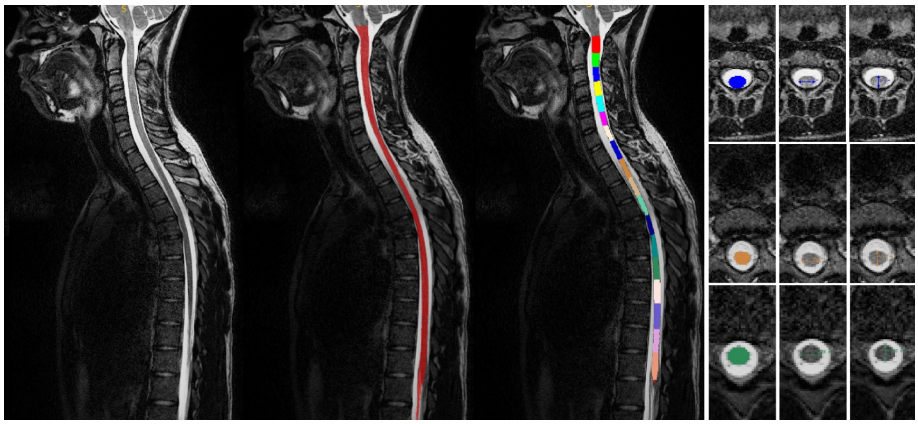

Figure 12: T2-Weighted MRI Analysis for Aim 1 – Spinal Cord Segmentation and CSA Measurements. From left to right: T2-weighted sagittal MRI, Automated spinal cord segmentation, Vertebral-level labeling from C1 to T11, CSA extraction along the spinal cord.

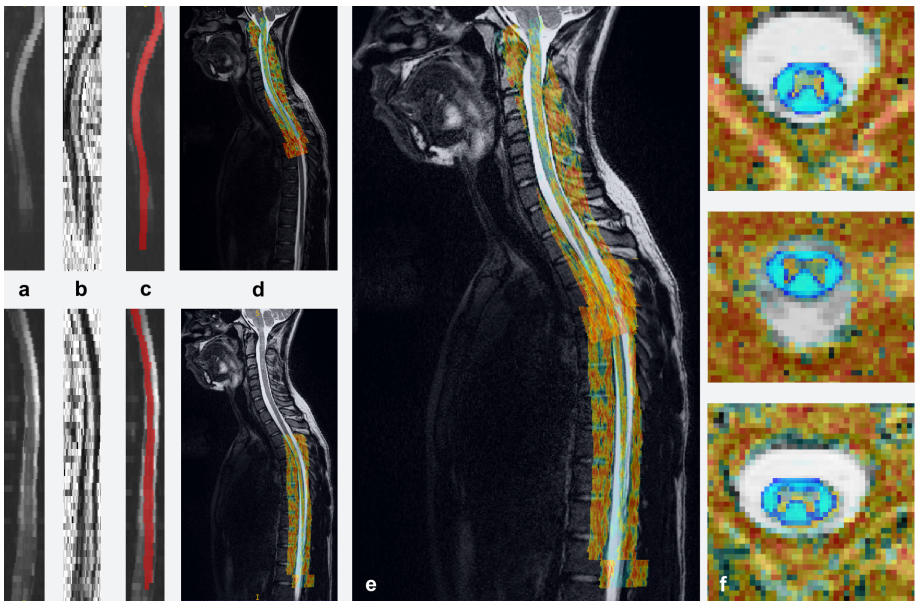

Figure 13: DTI Analysis for Aim 1 – FA Measurements in the Pediatric Spinal Cord. (a) Raw sagittal HYDI image. (b) Estimated FA map. (c) Automated spinal cord segmentation overlay. (d, e) FA map overlaid on T2-weighted MRI, highlighting microstructural features from C1 to T11. (f) Cross-sectional FA maps at different vertebral levels, with WM and GM segmentations used for extracting FA values in each region.

correlated with age at r = 0.49 ($p < 0.0001$) and RL width at r = 0.56 ($p < 0.00001$). Gender-based comparisons showed that males consistently exhibited larger CSA and RL widths. Notably, at C2, the RL width difference between males and females was statistically significant ($p = 0.033$), and similar trends were observed across neighboring levels. These findings emphasize the importance of considering both age and sex when establishing normative reference values for pediatric spinal cord morphology.

Figure 14 illustrates the average CSA, AP width, and RL width of the spinal cord across vertebral levels, stratified by gender. The analysis included 72 female and 55 male subjects, with average ages of 12.66 ± 3.40 and 12.32 ± 3.23 years, respectively. Across nearly all vertebral levels, males exhibited slightly larger structural measurements than females, particularly in the cervical and upper thoracic regions. This trend is most pronounced in the CSA and RL measurements, where the male group showed visibly higher values than females, especially between C1 and C6. The

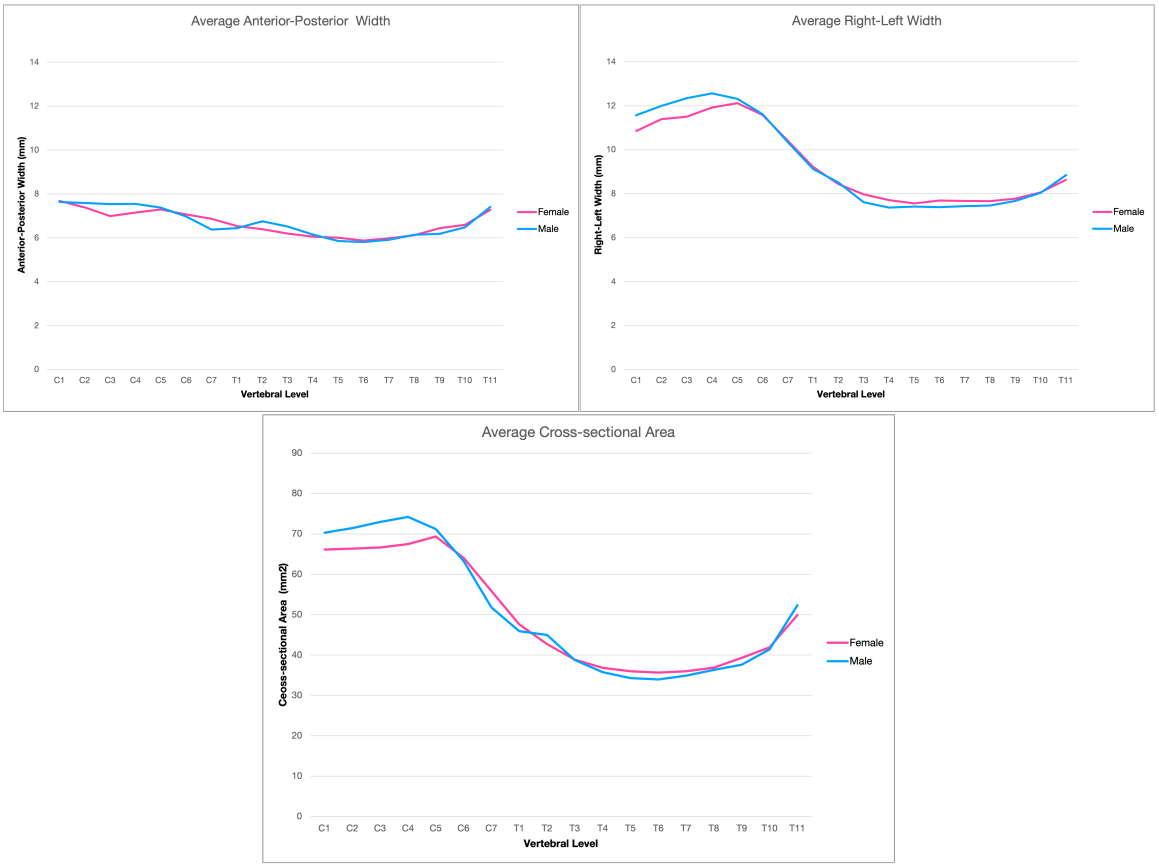

Figure 14: Gender-based comparison of spinal cord structural measures across vertebral levels. The plots show the average AP width, RL width, and CSA of the spinal cord for male (n = 55) and female (n = 72) pediatric participants.

AP width showed a less consistent but still slightly elevated pattern in males. The CSA plot reveals a characteristic dip in values around the cervicothoracic junction (C6–T1), followed by a gradual increase in the thoracic levels, consistent with known anatomical transitions. The RL diameter plot exhibits similar anatomical curvature, with peak widths in upper cervical regions and narrowing in thoracic segments.

Moving forward, we will continue collecting data to reach a total of 150 TD subjects. Our focus will be on increasing the representation of 6- and 7-year-old children, as well as male subjects, to ensure a balanced dataset that captures early developmental changes in spinal cord morphology. Additional analyses will incorporate DKI, NODDI, and MT imaging to further characterize microstructural and myelin-

related changes in the spinal cord. Further investigation into age- and gender-specific variations in spinal cord biomarkers will be conducted by stratifying the cohort by biological sex and discrete age groups. Structural and microstructural MRI metrics will be compared across these subgroups to evaluate developmental trajectories and sex-based differences. To facilitate reproducibility, all de-identified imaging-derived features and associated demographic variables will be made publicly available upon study completion and publication.

Aim 2: Machine Learning-Based Classification of Pediatric SCI Severity

To assess spinal cord injury severity in pediatric patients, we have collected MRI data from 25 SCI subjects, in addition to the TD cohort. These data allow for direct comparisons between injured and healthy spinal cords, facilitating the extraction of discriminative imaging biomarkers for machine learning applications. Structural and diffusion metrics from T2-weighted and DTI imaging were analyzed to assess differences between TD and SCI subjects. Initial analyses revealed significant reductions in CSA and FA in SCI subjects indicating compromised microstructural integrity.

A deep learning-based classification model was developed using 60 TD and 20 SCI subjects to distinguish SCI severity based on T2-weighted MRI features. We implemented a CNN-based model trained on extracted spinal cord structural features, including CSA, RL width, and AP width. The CNN architecture, illustrated in Figure 15, consists of multiple convolutional layers for feature extraction, followed by fully connected layers and a final softmax classification layer. The model was trained using the Adam optimizer, with categorical weighted cross-entropy as the loss function. Training was performed for 50 epochs with early stopping to prevent overfitting, using an 80-20 train-test split.

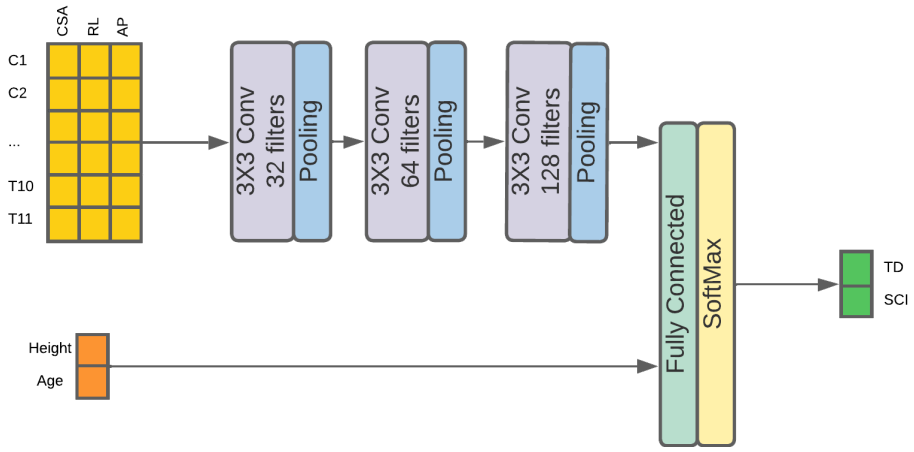

Figure 15: CNN architecture used for pediatric SCI classification. The model consists of three convolutional layers (3×3 kernel) with increasing filter sizes (32, 64, and 128), each followed by max pooling. Extracted features are passed through fully connected layers and a softmax classifier for final prediction.

Although the number of SCI subjects is limited, we took multiple steps to mitigate overfitting and ensure generalizability. We used a relatively lightweight architecture (with near $40K$ parameters), incorporated early stopping, and monitored both training and validation loss to avoid overfitting. The loss function was weighted to account for class imbalance, and the data split (80–20) ensured that test samples were entirely unseen during training.

To evaluate the CNN's performance, we compared it against traditional machine learning classifiers, including RF and SVM. These models were trained on the same extracted spinal cord features without deep feature learning. Model performance was assessed using accuracy, sensitivity, specificity, and F1-score. The CNN model significantly ($p < 0.05$) outperformed traditional classifiers, achieving an accuracy of 96.59% (95% CI: 94.50%–98.68%) in distinguishing SCI from TD subjects. In contrast, the Random Forest and SVM models achieved 85.32% and 89.47% accuracy, respectively. The CNN also demonstrated superior sensitivity (94.87%) and specificity (97.89%), highlighting its ability to effectively classify pediatric SCI. The results indicate that deep learning captures complex spatial dependencies in spinal cord

morphology that traditional models are unable to leverage.

Building on this binary classification, we extended the model to a clinically relevant three-class problem: TD, motor complete (AIS A/B) SCI , and motor incomplete (AIS C/D) SCI. Using the same CNN architecture and spinal cord features, the model achieved 94.92% accuracy (95% CI: 92.10%–97.74%) on the test set. The model demonstrated strong performance across all severity categories, including near-perfect precision for AIS A and B groups, and substantially outperformed traditional models, including Random Forest (74.00%) and SVM (68.89%).

These results highlight the value of spinal cord structural features as biomarkers for SCI severity and demonstrate the power of CNNs in modeling these complex spatial relationships. Future work will focus on integrating additional imaging modalities, particularly diffusion and microstructural metrics from DTI, to further improve severity prediction and generalizability.

Aim 3: Preprocessing of Acute Adult SCI Data for Classification

To facilitate automated severity classification in acute adult SCI, we have completed comprehensive data preprocessing on MRI scans from 190 adult SCI subjects. This preprocessing ensures high-quality, standardized inputs for deep learning models by addressing image artifacts, aligning structural and diffusion images, and extracting relevant biomarkers.

The preprocessing pipeline began with motion correction to minimize artifacts in diffusion-weighted images, ensuring consistency in DTI-derived metrics. Following motion correction, segmentation and vertebral labeling were performed using the Spinal Cord Toolbox (SCT), enabling accurate localization of spinal levels from C1 to T11. After segmentation, DTI parameter estimation was conducted to generate FA,

MD, AD, and RD maps, providing diffusion-based insights into spinal cord integrity. These maps were then coregistered with T2-weighted images to align structural and microstructural data spatially, ensuring multimodal consistency across subjects. Finally, a rigorous quality control process was implemented to verify segmentation accuracy and diffusion metric integrity, removing any low-quality scans that could compromise classification performance.

The completion of this preprocessing pipeline has resulted in a high-quality dataset, ready for deep learning-based severity assessment. This dataset will serve as the foundation for training classification models capable of distinguishing between different levels of SCI severity. The next step involves integrating this dataset into a multi-modal learning framework, incorporating both T2-weighted and DTI metrics to develop models for predicting AIS severity categories in acute SCI patients.

Future Work

Building upon the preliminary findings, future work will focus on expanding data collection, developing machine learning models, and integrating multimodal MRI data. The planned research directions are outlined in Table 1, which presents the structured timeline for completing the remaining research tasks. For Aim 1, data collection will continue until October 2025, with image preprocessing occurring simultaneously. After October 2025, we will begin benchmark generation and the establishment of normative values based on extracted biomarkers. This will be followed by statistical analysis to identify age, height, and gender-related patterns in spinal cord biomarkers. We expect to complete this aim by November 2025.

For Aim 2, while data collection for Aim 1 continues, we will begin developing machine learning models using the currently available data for both TD vs. SCI classification and SCI severity prediction, starting in July 2025. This initial development phase will allow us to have a functional model ready by the time data collection is

Table 1. Proposed Timeline for PhD Dissertation

Task Description	Mar	Apr	May	Jun	Jul	Aug	Sep	Oct	Nov	Des	Jan	Feb	Mar	Apr	May
Proposal	X	X	X												
Proposal Presentation															
Address feedback from the proposal committee															
Submit final proposal document															
Aim 1: Pediatric Data Collection & Analysis	X	X	X	X	X	X	X	X	X						
Pediatric Data Collection															
Pediatric Data Analysis															
Statistical Analysis															
Aim 2: Pediatric Model Development & Testing					X	X	X	X	X	X					
Model Development and Testing on Collected Data															
Final Development and Testing on the Whole Data															
Aim 3: Adult Deep Learning Model Implementation	X	X	X	X	X	X									
Baseline Models Development (Simple CNN / Single Modality)															
Baseline Models Development (Simple CNN / Multimodal)															
Proposed Models Development															
Writing & Finalization							X	X	X	X	X	X	X	X	X
Thesis Drafting															
Revision & Feedback															
Defend Thesis															
Incorporate Final Corrections & Submit Thesis															

complete. Once the full dataset is available, we will retrain and further improve the model using the complete data. We expect to complete this aim by January 2026.

In Aim 3, the primary focus will be on a stepwise model development approach for acute adult SCI severity classification. Initially, we will develop simple, single-modality baseline models, starting with CNN-based architectures trained on T2-weighted and DTI images separately. Once these models are established, the next phase will involve multimodal integration, combining structural and diffusion images to improve predictive performance. Finally, we will develop advanced models incorporating attention mechanisms and convolutional autoencoders for multimodal SCI severity classification. We expect to complete this aim by September 2025.

The final phase of the dissertation will focus on thesis writing, revisions, and defense preparation. Thesis drafting will begin in September 2025, with results from each aim progressively integrated as they are finalized. Revisions and feedback will

start in December 2025, ensuring continuous refinement. The final defense is expected to take place in March 2026, followed by necessary revisions and submission.

Publications

The following publications have resulted from the research conducted so far as part of this PhD work:

Journal and Conference Papers

1. **Sadeghi-Adl, Z.**, Naghizadehkashani, S., Middleton, D., Krisa, L., Alizadeh, M., Flanders, A. E., Faro, S. H., Wang, Z., Mohamed, F. B. (2025). Severity classification of pediatric spinal cord injuries using structural MRI measures and deep learning: A comprehensive analysis across all vertebral levels. *American Journal of Neuroradiology* (Accepted).

2. Naghizadeh Kashani, S., Vel, I., **Sadeghi-Adl, Z.**, Shahrampour, S., Middleton, D., Alizadeh, M., Krisa, L., Faro, S., Tounekti, S., Cohen-Adad, J., Mohamed, F. B. (2025). Magnetization transfer ratio in the typically developing pediatric spinal cord: Normative data and age correlation. *Journal of Neuroimaging*, 35(1), e70019.

3. Ahmad, F., **Sadeghi-Adl, Z.**, Hagen, C., Hiremath, S., Uhl, A., Ferretti, L., McCallion, P. (2024). Gait pattern analysis of older adults via radar micro-Doppler signatures and wrist-worn accelerometer data. In *Radar Sensor Technology XXVIII*, Proc. SPIE 13048, 180–184.

4. **Sadeghi-Adl, Z.**, Ahmad, F. (2023). Whitening-aided learning from radar micro-Doppler signatures for human activity recognition. *Sensors*, 23(17), 7486.

5. **Sadeghi-Adl, Z.**, Ahmad, F. (2023). Radar-based whitening-aided human activity recognition. In *Proceedings of the IEEE Radar Conference (RadarConf23)* (pp. 1–5).

6. **Sadeghi-Adl, Z.**, Ahmad, F. (2023). Semi-supervised convolutional autoencoder with attention mechanism for activity recognition. In *Proceedings of the 31st European Signal Processing Conference (EUSIPCO)* (pp. 785–789).

Conference Abstracts and Posters

7. **Sadeghi-Adl, Z.**, Naghizadehkashani, S., Raimondo, C., Middleton, D., Krisa, L., Alizadeh, M., Flanders, A. E., Faro, S. H., Mohamed, F. B. (2024, November). Structural assessment and ASIA impairment scale prediction in pediatric spinal cord injuries: Integrating imaging parameters and deep learning methods. Poster presented at the *RSNA 2024 Annual Meeting*, Chicago, IL.

8. **Sadeghi-Adl, Z.**, Naghizadehkashani, S., Krisa, L., Middleton, D., Alizadeh, M., Flanders, A. E., Faro, S. H., Mohamed, F. B. (2025). Deep learning-driven prediction of pediatric spinal cord injury severity using comprehensive structural MRI analysis. Abstract accepted at *ISMRM 2025* and *ASNR 2025*.

9. Naghizadehkashani, S., Alizadeh, M., Talekar, K., Middleton, D., Tammiraju, S., **Sadeghi-Adl, Z.**, Monadi, S., Faro, S., Mohamed, F. (2025). Exploring neural alterations in patients with tumor-related language deficits using graph theory measures: A resting-state fMRI study. Abstract accepted at *ISMRM 2025* and *ASNR 2025*.

10. Naghizadehkashani, S., Shoraka, O., Talekar, K., Middleton, D., **Sadeghi-Adl, Z.**, Faro, S., Mohamed, F., Alizadeh, M. (2025). Exploring neural dynamics: How visual disturbances and hallucinations impact dynamic brain connectivity in Parkinson's disease. Abstract accepted at *ASNR 2025*.

11. Suresh, S., Middleton, D., Thippeswamy, P. B., Ramachandran, K., Talekar, K., **Sadeghi-Adl, Z.**, Krisa, L., Shanmuganathan, R., Mohamed, F. (2025). Pre- and postoperative cross-sectional and diffusion measurements distal from spinal cord injury site. Abstract accepted at *ASNR 2025*.

CHAPTER 5

Conclusion

This proposal presents a novel approach to SCI assessment by integrating advanced MRI techniques and machine learning models across pediatric and adult populations. It is structured around three specific aims, each addressing critical gaps in SCI evaluation: establishing a pediatric normative MRI biomarker database, developing a machine learning-based severity classification framework for pediatric SCI, and creating an automated severity assessment model for acute adult SCI using multimodal MRI.

The first aim pioneers the development of the first pediatric spinal cord MRI biomarker database, filling the gap in standardized reference values. This dataset will provide a critical foundation for early diagnosis and monitoring of pediatric SCI. The second aim introduces the first machine learning approach to pediatric SCI severity classification. Traditional assessments like AIS suffer from subjectivity, whereas this study employs deep learning models for automated classification. The third aim advances acute adult SCI assessment by developing the first 3D multimodal deep learning model for severity grading. Unlike prior studies that rely on 2D image slices or single-modality approaches, this study processes full volumetric data from a large acute adult SCI dataset.

This research addresses major gaps in SCI assessment by integrating multimodal MR imaging, machine learning, and objective severity prediction models. The preliminary results validate the feasibility of machine learning-based models for SCI classification and severity assessment, demonstrating superior performance compared

to traditional classifiers. The proposed methodologies will enhance SCI diagnosis, improve prognostic accuracy, and optimize treatment planning, reducing reliance on subjective clinical evaluations.

BIBLIOGRAPHY

[1] Hyun-Yoon Ko and Sungchul Huh. *Clinical and Functional Anatomy of the Spinal Cord*, pages 1–32. Springer Singapore, Singapore, 2021.

[2] Eric R Kandel, James H Schwartz, Thomas M Jessell, Steven Siegelbaum, A James Hudspeth, Sarah Mack, et al. *Principles of neural science*, volume 4. McGraw-hill New York, 2000.

[3] Arsalan Alizadeh, Scott Matthew Dyck, and Soheila Karimi-Abdolrezaee. Traumatic spinal cord injury: an overview of pathophysiology, models and acute injury mechanisms. *Frontiers in neurology*, 10:282, 2019.

[4] Emilio Moreno-González and Antonio Ibarra. The critical management of spinal cord injury: A narrative review. *Clinics and Practice*, 15(1), 2025.

[5] Emilio Moreno-González and Antonio Ibarra. The critical management of spinal cord injury: A narrative review. *Clinics and Practice*, 15(1):2, 2024.

[6] Miguel A Ortega, Oscar Fraile-Martinez, Cielo García-Montero, Sergio Haro, Miguel Ángel Álvarez-Mon, Diego De Leon-Oliva, Ana M Gomez-Lahoz, Jorge Monserrat, Mar Atienza-Pérez, David Díaz, et al. A comprehensive look at the psychoneuroimmunoendocrinology of spinal cord injury and its progression: mechanisms and clinical opportunities. *Military Medical Research*, 10(1):26, 2023.

[7] M Hales, E Biros, and JE Reznik. Reliability and validity of the sensory component of the international standards for neurological classification of spinal cord injury (isncsci): a systematic review. *Topics in Spinal Cord Injury Rehabilitation*, 21(3):241–249, 2015.

[8] Bizhan Aarabi, Charles A Sansur, David M Ibrahimi, J Marc Simard, David S Hersh, Elizabeth Le, Cara Diaz, Jennifer Massetti, and Noori Akhtar-Danesh. Intramedullary lesion length on postoperative magnetic resonance imaging is a strong predictor of asia impairment scale grade conversion following decompressive surgery in cervical spinal cord injury. *Neurosurgery*, 80(4):610–620, 2017.

[9] Ling Hu, Siyu Yang, Bo Jin, and Chao Wang. Advanced neuroimaging role in traumatic brain injury: A narrative review. *Frontiers in Neuroscience*, 16, 2022.

[10] Allan R Martin, Izabela Aleksanderek, Julien Cohen-Adad, Zenovia Tarmohamed, Lindsay Tetreault, Nathaniel Smith, David W Cadotte, Adrian Crawley, Howard Ginsberg, David J Mikulis, et al. Translating state-of-the-art spinal cord mri techniques to clinical use: A systematic review of clinical studies utilizing dti, mt, mwf, mrs, and fmri. *NeuroImage: Clinical*, 10:192–238, 2016.

[11] Ioannis Tsougos. *Advanced MR neuroimaging: from theory to clinical practice*. CRC Press, 2017.

[12] Suraj D Serai. Basics of magnetic resonance imaging and quantitative parameters t1, t2, t2*, t1rho and diffusion-weighted imaging. *Pediatric radiology*, 52(2):217–227, 2022.

[13] Roland Bammer. Basic principles of diffusion-weighted imaging. *European journal of radiology*, 45(3):169–184, 2003.

[14] Denis Le Bihan, Jean-François Mangin, Cyril Poupon, Chris A Clark, Sabina Pappata, Nicolas Molko, and Hughes Chabriat. Diffusion tensor imaging: concepts and applications. *Journal of Magnetic Resonance Imaging: An Official Journal of the International Society for Magnetic Resonance in Medicine*, 13(4):534–546, 2001.

[15] Hui Zhang, Torben Schneider, Claudia A Wheeler-Kingshott, and Daniel C Alexander. Noddi: practical in vivo neurite orientation dispersion and density imaging of the human brain. *Neuroimage*, 61(4):1000–1016, 2012.

[16] Jens H Jensen, Joseph A Helpern, Anita Ramani, Hanzhang Lu, and Kyle Kaczynski. Diffusional kurtosis imaging: the quantification of non-gaussian water diffusion by means of magnetic resonance imaging. *Magnetic Resonance in Medicine: An Official Journal of the International Society for Magnetic Resonance in Medicine*, 53(6):1432–1440, 2005.

[17] Robert S Balaban and TL Ceckler. Magnetization transfer contrast in magnetic resonance imaging. *Magnetic resonance quarterly*, 8(2):116–137, 1992.

[18] Yu-Chien Wu and Andrew L Alexander. Hybrid diffusion imaging. *NeuroImage*, 36(3):617–629, 2007.

[19] Andrew L Alexander, Yu-Chien Wu, and Pradeep C Venkat. Hybrid diffusion imaging (hydi). In *2006 International Conference of the IEEE Engineering in Medicine and Biology Society*, pages 2245–2248. IEEE, 2006.

[20] Antti Brander, Eerika Koskinen, Teemu M Luoto, Ullamari Hakulinen, Mika Helminen, Sirpa Savilahti, Pertti Ryymin, Prasun Dastidar, and Juha Öhman. Diffusion tensor imaging of the cervical spinal cord in healthy adult population: normative values and measurement reproducibility at 3t mri. *Acta Radiologica*, 55(4):478–485, 2014.

[21] S Saksena, DM Middleton, L Krisa, P Shah, SH Faro, R Sinko, J Gaughan, J Finsterbusch, MJ Mulcahey, and FB Mohamed. Diffusion tensor imaging of the normal cervical and thoracic pediatric spinal cord. *American Journal of Neuroradiology*, 37(11):2150–2157, 2016.

[22] Natalia SC Cunha, Anahita Malvea, Sarah Sadat, George M Ibrahim, and Michael G Fehlings. Pediatric spinal cord injury: a review. *Children*, 10(9):1456, 2023.

[23] Michael J DeVivo and Lawrence C Vogel. Epidemiology of spinal cord injury in chiloren and adolescents. *The Journal of Spinal Cord Medicine*, 27(sup1):S4–S10, 2004.

[24] G Savic, EMK Bergström, HL Frankel, MA Jamous, and PW Jones. Inter-rater reliability of motor and sensory examinations performed according to american spinal injury association standards. *Spinal cord*, 45(6):444–451, 2007.

[25] Yunus Ziya Arslan, Rustu Murat Demirer, Deniz Palamar, Mukden Ugur, and Safak Sahir Karamehmetoglu. Comparison of the data classification approaches to diagnose spinal cord injury. *Computational and Mathematical Methods in Medicine*, 2012(1):803980, 2012.

[26] Bunheang Tay, Jung Keun Hyun, and Sejong Oh. A machine learning approach for specification of spinal cord injuries using fractional anisotropy values obtained from diffusion tensor images. *Computational and mathematical methods in medicine*, 2014(1):276589, 2014.

[27] I. Gusti Lanang Ngurah Agung Artha Wiguna, Yosi Kristian, Maria Florencia Deslivia, Rudi Limantara, David Cahyadi, Ivan Alexander Liando, Hendra Aryudi Hamzah, Kevin Kusuman, Dominicus Dimitri, Maria Anastasia, et al. A deep learning approach for cervical cord injury severity determination through axial and sagittal magnetic resonance imaging segmentation and classification. *European Spine Journal*, 33(11):4204–4213, 2024.

[28] Henry Gray. *Anatomy of the human body*, volume 8. Lea & Febiger, 1878.

[29] J Gordon Betts, Kelly A Young, James A Wise, Eddie Johnson, Brandon Poe, Dean H Kruse, Oksana Korol, Jody E Johnson, Mark Womble, and Peter DeSaix. *Anatomy and physiology 2e*. 2024.

[30] Christopher S Ahuja, Jefferson R Wilson, Satoshi Nori, Mark Kotter, Claudia Druschel, Armin Curt, and Michael G Fehlings. Traumatic spinal cord injury. *Nature reviews Disease primers*, 3(1):1–21, 2017.

[31] Gerhard Werner and Barry L Whitsel. The topology of dermatomal projection in the medial lemniscal system. *The Journal of physiology*, 192(1):123–144, 1967.

[32] Laurence Ge, Karan Arul, Tochukwu Ikpeze, Avionna Baldwin, Jean L Nickels, and Addisu Mesfin. Traumatic and nontraumatic spinal cord injuries. *World neurosurgery*, 111:e142–e148, 2018.

[33] National Spinal Cord Injury Statistical Center. Spinal cord injury facts and figures at a glance. `https://msktc.org/sites/default/files/Facts-and-Figures-2024-Eng-508.pdf`, 2024. University of Alabama at Birmingham.

[34] Michael J DeVivo. Epidemiology of spinal cord injury. *Spinal Cord Medicine Principles and Practice. Demos Medical Publishing: New York, NY*, pages 78–84, 2010.

[35] Steven C Kirshblum, Stephen P Burns, Fin Biering-Sorensen, William Donovan, Daniel E Graves, Amitabh Jha, Mark Johansen, Linda Jones, Andrei Krassioukov, MJ Mulcahey, et al. International standards for neurological classification of spinal cord injury (revised 2011). *The journal of spinal cord medicine*, 34(6):535–546, 2011.

[36] Ray Hashman Hashemi, William G Bradley, and Christopher J Lisanti. *MRI: the basics: The Basics*. Lippincott Williams & Wilkins, 2012.

[37] Gabriela Trifan, Ramtilak Gattu, Ewart Mark Haacke, Zhifeng Kou, and Randall R Benson. Mr imaging findings in mild traumatic brain injury with persistent neurological impairment. *Magnetic resonance imaging*, 37:243–251, 2017.

[38] Derek K Jones. *Diffusion mri*. Oxford University Press, 2010.

[39] Devon M Middleton and Chris J Conklin. Advanced diffusion imaging in neuroradiology. In *Functional Neuroradiology: Principles and Clinical Applications*, pages 933–947. Springer, 2023.

[40] N C Silver, C D Good, G J Barker, D G MacManus, A J Thompson, I F Moseley, W I McDonald, and D H Miller. Sensitivity of contrast enhanced mri in multiple sclerosis. effects of gadolinium dose, magnetization transfer contrast and delayed imaging. *Brain*, 120(7):1149–1161, 07 1997.

[41] Alex Zwanenburg, Martin Vallières, Mahmoud A Abdalah, Hugo JWL Aerts, Vincent Andrearczyk, Aditya Apte, Saeed Ashrafinia, Spyridon Bakas, Roelof J Beukinga, Ronald Boellaard, et al. The image biomarker standardization initiative: standardized quantitative radiomics for high-throughput image-based phenotyping. *Radiology*, 295(2):328–338, 2020.

[42] S Kevin Zhou, Hayit Greenspan, Christos Davatzikos, James S Duncan, Bram Van Ginneken, Anant Madabhushi, Jerry L Prince, Daniel Rueckert, and Ronald M Summers. A review of deep learning in medical imaging: Imaging traits, technology trends, case studies with progress highlights, and future promises. *Proceedings of the IEEE*, 109(5):820–838, 2021.

[43] Mayank Arya Chandra and SS Bedi. Survey on svm and their application in image classification. *International Journal of Information Technology*, 13(5):1–11, 2021.

[44] Feon Jaison, Viiay Kumar Pandey, and Ashish Bishnoi. Developing support vector machines for accurate medical image analysis. In *2024 International Conference on Optimization Computing and Wireless Communication (ICOCWC)*, pages 1–7, 2024.

[45] Tanvi Gupta, Pranay Manocha, Tapan K Gandhi, RK Gupta, and Bijaya K Panigrahi. Tumor classification and segmentation of mr brain images. *arXiv preprint arXiv:1710.11309*, 2017.

[46] Mohd Fauzi Bin Othman, Noramalina Bt Abdullah, and Nurul Fazrena Bt Kamal. Mri brain classification using support vector machine. In *2011 Fourth International Conference on Modeling, Simulation and Applied Optimization*, pages 1–4, 2011.

[47] Shan Suthaharan. Decision tree learning. *Machine Learning Models and Algorithms for Big Data Classification: Thinking with Examples for Effective Learning*, pages 237–269, 2016.

[48] Steven J Rigatti. Random forest. *Journal of Insurance Medicine*, 47(1):31–39, 2017.

[49] Zhe Ma, Bin Jing, Yuxia Li, Huagang Yan, Zhaoxia Li, Xiangyu Ma, Zhizheng Zhuo, Lijiang Wei, Haiyun Li, Alzheimer's Disease Neuroimaging Initiative, et al. Identifying mild cognitive impairment with random forest by integrating multiple mri morphological metrics. *Journal of Alzheimer's Disease*, 73(3):991–1002, 2020.

[50] Wei Pei, Chen Wang, Hai Liao, Xiaobo Chen, Yunyun Wei, Xia Huang, Xueli Liang, Huayan Bao, Danke Su, and Guanqiao Jin. Mri-based random survival forest model improves prediction of progression-free survival to induction chemotherapy plus concurrent chemoradiotherapy in locoregionally advanced nasopharyngeal carcinoma. *BMC cancer*, 22(1):739, 2022.

[51] Nicholas Dietz, Vaitheesh Jaganathan, Victoria Alkin, Jersey Mettille, Maxwell Boakye, and Doniel Drazin. Machine learning in clinical diagnosis, prognostication, and management of acute traumatic spinal cord injury (sci): A systematic review. *Journal of Clinical Orthopaedics and Trauma*, 35:102046, 2022.

[52] Keiron O'shea and Ryan Nash. An introduction to convolutional neural networks. *arXiv preprint arXiv:1511.08458*, 2015.

[53] Jin Liu, Yi Pan, Min Li, Ziyue Chen, Lu Tang, Chengqian Lu, and Jianxin Wang. Applications of deep learning to mri images: A survey. *Big Data Mining and Analytics*, 1(1):1–18, 2018.

[54] Amir Ebrahimi, Suhuai Luo, and for the Alzheimer's Disease Neuroimaging Initiative. Convolutional neural networks for alzheimer's disease detection on mri images. *Journal of Medical Imaging*, 8(2):024503–024503, 2021.

[55] Gongbo Liang, Xin Xing, Liangliang Liu, Yu Zhang, Qi Ying, Ai-Ling Lin, and Nathan Jacobs. Alzheimer's disease classification using 2d convolutional neural networks. In *2021 43rd annual international conference of the ieee engineering in medicine & biology society (embc)*, pages 3008–3012. IEEE, 2021.

[56] Mahdieh Shabanian, Markus Wenzel, and John P DeVincenzo. Infant brain age classification: 2d cnn outperforms 3d cnn in small dataset. In *Medical Imaging 2022: Image Processing*, volume 12032, pages 626–633. SPIE, 2022.

[57] Mohammad Hamghalam, Baiying Lei, and Tianfu Wang. Convolutional 3d to 2d patch conversion for pixel-wise glioma segmentation in mri scans. In *International MICCAI Brainlesion Workshop*, pages 3–12. Springer, 2019.

[58] Satya P Singh, Lipo Wang, Sukrit Gupta, Haveesh Goli, Parasuraman Padmanabhan, and Balázs Gulyás. 3d deep learning on medical images: a review. *Sensors*, 20(18):5097, 2020.

[59] Hiba Mzoughi, Ines Njeh, Ali Wali, Mohamed Ben Slima, Ahmed BenHamida, Chokri Mhiri, and Kharedine Ben Mahfoudhe. Deep multi-scale 3d convolutional neural network (cnn) for mri gliomas brain tumor classification. *Journal of Digital Imaging*, 33:903–915, 2020.

[60] Linmin Pei, Lasitha Vidyaratne, Wei-Wen Hsu, Md Monibor Rahman, and Khan M Iftekharuddin. Brain tumor classification using 3d convolutional neural network. In *Brainlesion: Glioma, Multiple Sclerosis, Stroke and Traumatic Brain Injuries: 5th International Workshop, BrainLes 2019, Held in Conjunction with MICCAI 2019, Shenzhen, China, October 17, 2019, Revised Selected Papers, Part II 5*, pages 335–342. Springer, 2020.

[61] A Vaswani. Attention is all you need. *Advances in Neural Information Processing Systems*, 2017.

[62] Arindam Halder, Sanghita Gharami, Priyangshu Sadhu, Pawan Kumar Singh, Marcin Woźniak, and Muhammad Fazal Ijaz. Implementing vision transformer for classifying 2d biomedical images. *Scientific Reports*, 14(1):12567, 2024.

[63] Yin Dai, Yifan Gao, and Fayu Liu. Transmed: Transformers advance multimodal medical image classification. *Diagnostics*, 11(8):1384, 2021.

[64] Xiangyi Yan, Hao Tang, Shanlin Sun, Haoyu Ma, Deying Kong, and Xiaohui Xie. After-unet: Axial fusion transformer unet for medical image segmentation. In *Proceedings of the IEEE/CVF winter conference on applications of computer vision*, pages 3971–3981, 2022.

[65] Ali Hatamizadeh, Yucheng Tang, Vishwesh Nath, Dong Yang, Andriy Myronenko, Bennett Landman, Holger R Roth, and Daguang Xu. Unetr: Transformers for 3d medical image segmentation. In *Proceedings of the IEEE/CVF winter conference on applications of computer vision*, pages 574–584, 2022.

[66] Shehan Perera, Pouyan Navard, and Alper Yilmaz. Segformer3d: an efficient transformer for 3d medical image segmentation. In *Proceedings of the IEEE/CVF Conference on Computer Vision and Pattern Recognition*, pages 4981–4988, 2024.

[67] DB McCoy, SM Dupont, C Gros, Julien Cohen-Adad, RJ Huie, A Ferguson, X Duong-Fernandez, LH Thomas, V Singh, J Narvid, et al. Convolutional neural network–based automated segmentation of the spinal cord and contusion injury: Deep learning biomarker correlates of motor impairment in acute spinal cord injury. *American Journal of Neuroradiology*, 40(4):737–744, 2019.

[68] Enamundram Naga Karthik, Jan Valošek, Andrew C Smith, Dario Pfyffer, Simon Schading-Sassenhausen, Lynn Farner, Kenneth A Weber, Patrick Freund, and Julien Cohen-Adad. Sciseg: Automatic segmentation of intramedullary lesions in spinal cord injury on t2-weighted mri scans. *Radiology: Artificial Intelligence*, 7(1):e240005, 2024.

[69] Sho Okimatsu, Satoshi Maki, Takeo Furuya, Takayuki Fujiyoshi, Mitsuhiro Kitamura, Taigo Inada, Masaaki Aramomi, Tomonori Yamauchi, Takuya Miyamoto, Takaki Inoue, et al. Determining the short-term neurological prognosis for acute cervical spinal cord injury using machine learning. *Journal of Clinical Neuroscience*, 96:74–79, 2022.

[70] Yann Facchinello, Marie Beauséjour, Andréane Richard-Denis, Cynthia Thompson, and Jean-Marc Mac-Thiong. Use of regression tree analysis for predicting the functional outcome after traumatic spinal cord injury. *Journal of neurotrauma*, 38(9):1285–1291, 2021.

[71] Nadja Kadom, Kartik Reddy, Maxwell E Cooper, Jack Knight-Scott, Richard A Jones, and Susan Palasis. Diagnostic excellence in pediatric spine imaging: Using contextualized imaging protocols. *Diagnostics*, 13(18):2973, 2023.

[72] Julien Cohen-Adad, Eva Alonso-Ortiz, Mihael Abramovic, Carina Arneitz, Nicole Atcheson, Laura Barlow, Robert L Barry, Markus Barth, Marco Battiston, Christian Büchel, et al. Open-access quantitative mri data of the spinal cord and reproducibility across participants, sites and manufacturers. *Scientific Data*, 8(1):219, 2021.

[73] Mary Jane Mulcahey, John Gaughan, Randal R Betz, and KJ Johansen. The international standards for neurological classification of spinal cord injury: reliability of data when applied to children and youths. *Spinal Cord*, 45(6):452–459, 2007.

[74] Sangyoon Lee, Francesca Branzoli, Thanh Nguyen, Ovidiu Andronesi, Alexander Lin, Roberto Liserre, Gerd Melkus, Clark Chen, Małgorzata Marjańska, and Patrick J. Bolan. A Deep Learning Approach for Placing Magnetic Resonance Spectroscopy Voxels in Brain Tumors . In *Medical Image Computing and Computer Assisted Intervention – MICCAI 2024*, volume LNCS 15003, pages 543 – 552. Springer Nature Switzerland, October 2024.

[75] Qiming Cui, Duygu Tosun, Pratik Mukherjee, and Reza Abbasi-Asl. 7T MRI Synthesization from 3T Acquisitions . In *Medical Image Computing and Computer Assisted Intervention – MICCAI 2024*, volume LNCS 15007, pages 35 – 44. Springer Nature Switzerland, October 2024.

[76] Faezeh Vedaei, Najmeh Mashhadi, Mahdi Alizadeh, George Zabrecky, Daniel Monti, Nancy Wintering, Emily Navarreto, Chloe Hriso, Andrew B Newberg, and Feroze B Mohamed. Deep learning-based multimodality classification of chronic mild traumatic brain injury using resting-state functional mri and pet imaging. *Frontiers in Neuroscience*, 17:1333725, 2024.

[77] Benjamin De Leener, Simon Lévy, Sara M Dupont, Vladimir S Fonov, Nikola Stikov, D Louis Collins, Virginie Callot, and Julien Cohen-Adad. Sct: Spinal cord toolbox, an open-source software for processing spinal cord mri data. *Neuroimage*, 145:24–43, 2017.

[78] Benjamin De Leener, Vladimir S Fonov, D Louis Collins, Virginie Callot, Nikola Stikov, and Julien Cohen-Adad. Pam50: Unbiased multimodal template of the brainstem and spinal cord aligned with the icbm152 space. *Neuroimage*, 165:170–179, 2018.

[79] Julien Cohen-Adad, S Levy, and B Avants. Slice-by-slice regularized registration for spinal cord mri: Slicereg. In *Proceedings of the International Society for Magnetic Resonance in Medicine 23rd Annual Meeting and Exhibition, Toronto, Canada*, 2015.